Electronic Supplementary Material (ESI) for Soft Matter.

Supplemental data: Simulated filament shapes in embedded 3D printing*

Leanne M. Friedrich, Jonathan E. Seppala

National Institute of Standards and Technology

November 18, 2021

Contents

List of Figures

*Official contribution of the National Institute of Standards and Technology; not subject to copyright in the United States.

S1 Boundary conditions

Initial boundary condition files for U (velocity), p_rgh (pressure), and alpha.ink (volume fraction of ink), setting the atmosphere boundary as a quasi-free surface, are shown below. Note that the dimensions vector indicates the units of the variable as [kg, m, s, ...]. For example, the units of p_rgh are $kg/(m * s^2)$.

U

```
FoamFile
{
    version     2.0;
    format      ascii;
    class       volVectorField;
    object      U;
}
// * * * * * * * * * * * * * * * * * * * * * * * * * * * * * * * * * * * * * //;

dimensions  [0 1 -1 0 0 0 0];

internalField uniform (0 0 0);

boundaryField
{
  bathFlow
  {
    type  fixedValue;
    value uniform (0.01 0 0);
  }

  inkFlow
  {
    type  fixedValue;
    value uniform (0 0 -0.01);
  }

  atmosphere
  {
    type  pressureInletOutletVelocity;
    value uniform (0 0 0);
  }

  fixedWalls
  {
    type  noSlip;
  }

}
```

alpha.ink

```
FoamFile
{
    version     2.0;
    format      ascii;
    class       volScalarField;
    object      alpha.ink;
}
// * * * * * * * * * * * * * * * * * * * * * * * * * * * * * * * * * * * * * //;

dimensions  [0 0 0 0 0 0 0];

internalField uniform 0;

boundaryField
{
  bathFlow
  {
    type  fixedValue;
    value uniform 0;
  }

  inkFlow
  {
    type  fixedValue;
```

```
    value uniform 1;
  }

  atmosphere
  {
    type  inletOutlet;
    value uniform 0;
    inletValue  uniform 0;
  }

  fixedWalls
  {
    type  zeroGradient;
  }

}
```

p_rgh: quasi-free surface

```
FoamFile
{
    version     2.0;
    format      ascii;
    class       volScalarField;
    object      p_rgh;
}
// * * * * * * * * * * * * * * * * * * * * * * * * * * * * * * * * * * * * * //;

dimensions  [1 -1 -2 0 0 0 0];

internalField uniform 0;

boundaryField
{
  bathFlow
  {
    type  fixedFluxPressure;
    value uniform 0;
  }

  inkFlow
  {
    type  fixedFluxPressure;
    value uniform 0;
  }

  atmosphere
  {
    type  totalPressure;
    p0  uniform 0;
  }

  fixedWalls
  {
    type  fixedFluxPressure;
    value uniform 0;
  }

}
```

Alternatively, the atmosphere, which is on the top surface and downstream surface of the simulated volume, could be modeled as a zero gradient boundary, which would allow smooth continuity of the simulated volume into the bath, imposing a pressure condition that simulates a deep bath, instead of imposing a pressure condition that is more similar to a free surface. This can be done by modifying the pressure conditions, such that the atmosphere boundary will be defined as zeroGradient, rather than a total pressure of 0. Because this removes the reference pressure, a reference pressure must be established elsewhere in order to make these conditions solvable. We replace the fixedFluxPressure of 0 in the bathFlow condition with a totalPressure of

0. We also set the inkFlow pressure condition to a zeroGradient condition, rather than a fixedFluxPressure of 0, allowing smoother continuity of the pressure at the inlet.

p_rgh: deep bath

```
FoamFile
{
    version     2.0;
    format      ascii;
    class       volScalarField;
    object      p_rgh;
}
// * * * * * * * * * * * * * * * * * * * * * * * * * * * * * * * * * * * * * * //;

dimensions  [1 -1 -2 0 0 0 0];

internalField uniform 0;

boundaryField
{
  bathFlow
  {
    type  totalPressure;
    p0  uniform 0;
  }

  inkFlow
  {
    type  zeroGradient;
  }

  atmosphere
  {
    type  zeroGradient;
  }

  fixedWalls
  {
    type  fixedFluxPressure;
    value uniform 0;
  }

}
```

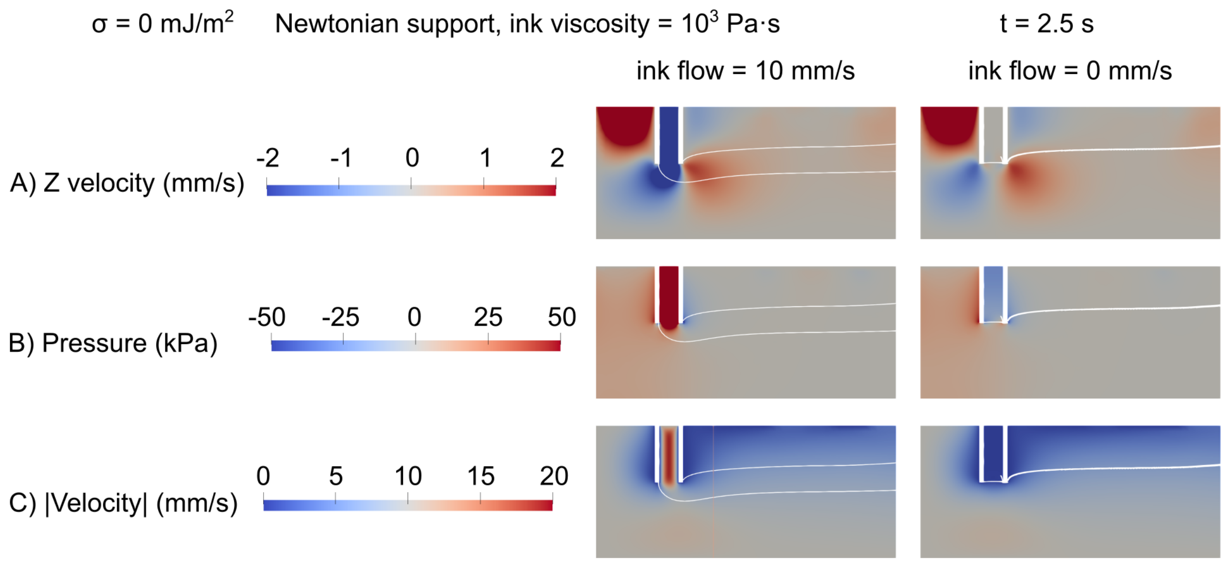

Figure S1: The flow field, with ink flow turned on and off, for the quasi-free surface atmosphere boundary. Dark red and blue regions are outside of the mapped color space. A) Vertical fluid velocity. B) Pressure, without hydrostatic pressure contribution. C) Magnitude of the fluid velocity.

Imposing the deep bath boundary condition alters the flow field and the filament shape, but it does not alter trends as a function of viscosity. Movement of the bath relative to the nozzle in the quasi-free surface case causes pressure and velocity gradients. At the bottom of the nozzle, support fluid flows downward upstream of the nozzle and upward downstream of the nozzle (Fig. S1A). At the top of the nozzle, support fluid flows upward upstream of the nozzle and downward downstream of the nozzle (Fig. S1A). This is accompanied by a pressure differential from the front to the back of the nozzle, where the pressure is positive upstream of the nozzle and negative downstream of the nozzle (Fig. S1B). A low-velocity wake follows the nozzle, regardless of ink flow.

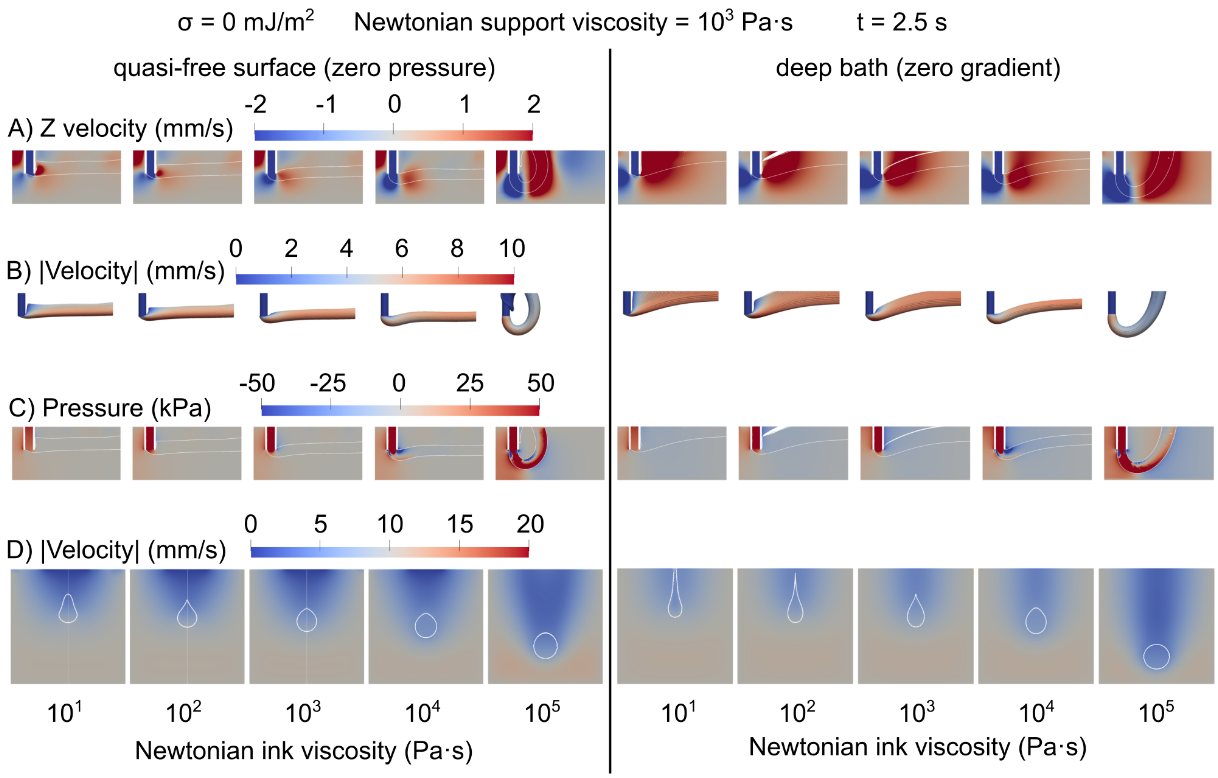

Figure S2: The flow field, for the quasi-free surface and deep bath boundary conditions, for Newtonian inks in Newtonian supports. Dark red and blue regions are outside of the mapped color space. A) Vertical fluid velocity. B) Ink-support interface, colored by velocity magnitude. C) Pressure, without hydrostatic pressure contribution. D) Magnitude of the fluid velocity, for a slice 1.5 mm behind the nozzle.

For Newtonian fluids, these flow patterns vary in the deep bath. In the deep bath, the downward flow downstream of the nozzle and the slow wake are diminished, and the upward flow region and negative pressure region downstream of the nozzle are much larger (Fig. S2A,C). Correspondingly, this exaggerates the defects described for the quasi-free surface. Upward displacement is much greater, and aspect ratios are much taller, in the deep bath (Fig. S2B,D). However, all of the trends remain the same. In both the quasi-free surface and the deep bath, upward displacement and vertical elongation increase with decreasing ink viscosity (Fig. S2B,D).

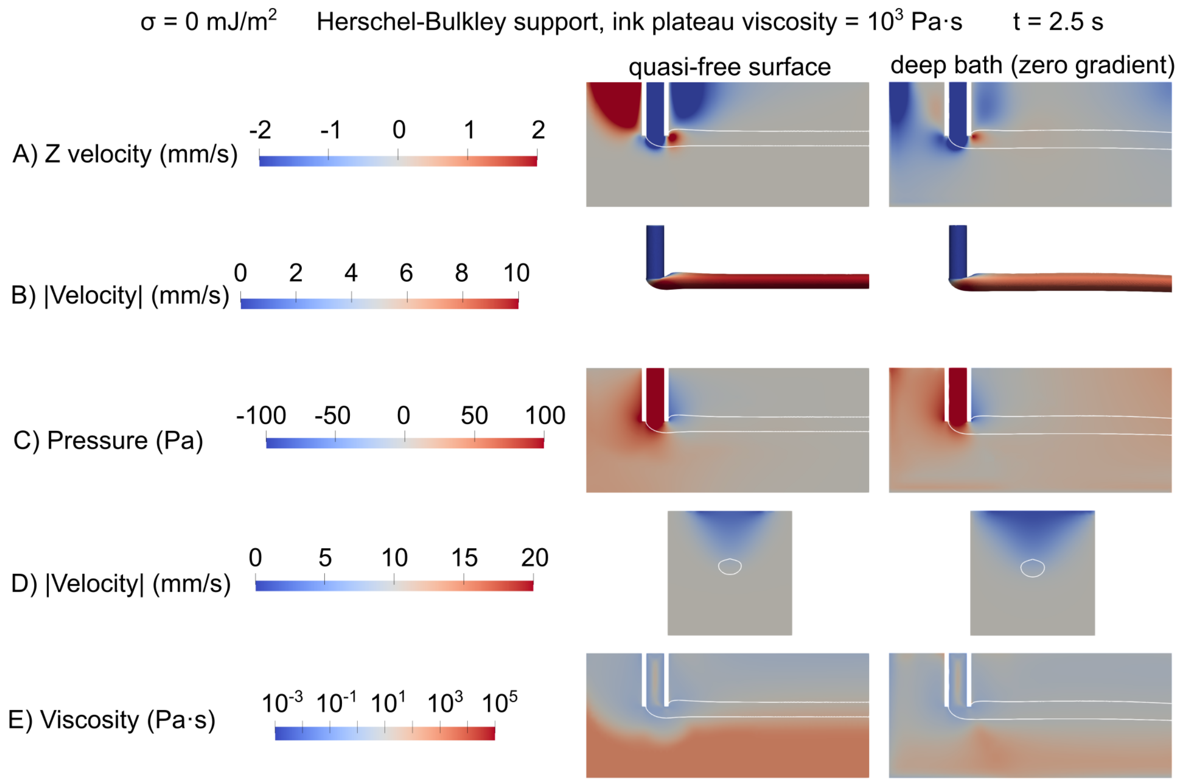

Figure S3: The flow field, for the quasi-free surface and deep bath boundary conditions, for Herschel-Bulkley inks in Herschel-Bulkley supports. Dark red and blue regions are outside of the mapped color space. A) Vertical fluid velocity. B) Ink-support interface, colored by velocity magnitude. C) Pressure, without hydrostatic pressure contribution. D) Magnitude of the fluid velocity, for a slice 1.5 mm behind the nozzle. E) Viscosity map.

For Herschel-Bulkley inks in Herschel-Bulkley supports, the deep bath has little effect on the filament shape, despite influencing the flow field (Fig. S3B). In the deep bath, the wake is wider (Fig. S3E), and the zero total pressure boundary condition on the front and bottom of the simulated volume create non-monotonic effects on the viscosity map, pressure map, and velocity map, indicating that the deep bath condition may be inappropriate for Herschel-Bulkley supports. In the quasi-free surface condition, the z velocity smoothly decreases toward the front of the bath, the pressure smoothly decreases toward the front and bottom of the bath, and the viscosity plateaus at the bottom and front of the bath (Fig. S3A,C,E). In contrast, in the deep bath condition, the z velocity increases, then flows strongly downward toward the front of the bath, the pressure decreases, the increases at the front and bottom of the bath, and the viscosity increases, then decreases at the front and bottom of the bath (Fig. S3A,C,E). Because the support is at a lower viscosity, the filament moves slower, worsening its $x - y$ positioning accuracy (Fig. S3B,E). This indicates that the zero total pressure condition on the front and bottom surface yields the support locally, which should not happen if those surfaces are meant to represent additional bath fluid.

While it is possible that this alternate boundary condition could better represent printing into a deep bath, the unusual z velocity field in Figure S3A and pressure field in Figure S3C indicate that this set of boundary conditions may not be accurate. Additionally, because all real baths reported so far are capped by a free surface, we choose to maintain the quasi-free surface for the remaining simulations.

S2 Rheology

$$\eta = min(\eta_0, \tau_0/\dot{\gamma} + k\dot{\gamma}^{n-1})$$

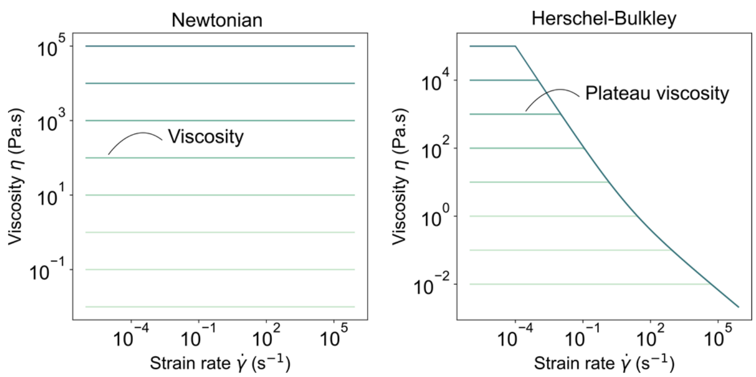

Figure S4: Viscosity vs. strain rate, for the simulated materials, where η_0 is the plateau viscosity, τ_0 is the yield stress, $\dot{\gamma}$ is the shear rate, k is the consistency index, and n is the flow index. τ_0 is set to 10 Pa, k is set to 3.75 Pa·s^n, and n is set to 0.45

Table S1: Reported rheological measurements in the literature, for embedded 3D printing inks and supports. Type indicates hydrophilicity (phil) or hydrobicity (phob). Model is Newtonian (N) or Herschel-Bulkley (HB), if reported. eta0 is the zero shear viscosity, tau0 is the yield stress, K is the HB consistency index, and n is the HB power law constant. In ref. [1], the inks have similar tau0, K, and n values to the supports.

	Ink			Support					
	Type	Model	eta0 (Pa*s)	Type	Model	eta0 (Pa*s)	tau0 (Pa)	K (Pa*s^n)	n
[2]	phil			phil	HB		29–43	5–10	0.47–0.73
[3]	phil			phil		10^2–10^3			
[4]	phil			phil	HB	44	5–136	44	0.3
[5]	phil			phil			1-80		
[6]	phil	N	1	phob	N	1			
[7]	phil	N	10^{-3}	phob	N	60			
[8]	phil			phil			0.25-3	6-10	0.25–0.5
[1]	phil	HB		phil	HB		1–2	1–5	0.29–0.51
[9]	phil			phob	HB		4–127	8–42	0.69–0.88
[10]	phil			phil			10–10^2		
[11]	phob			phil/phob emulsion			8–70		
[12]	phil			phil		10^3	2–40		
[13]	phil or phob			phil	HB		4–85		
[14]	phil		32	phil	HB	3×10^6			
[15]	phob	N	12.9	phob		10^5-10^7	4–80		
[16]	phob	N	1–10^2	phil	N	10^{-3}			
[17]	phil	N	10^{-2}–1	phil	HB		10–10^2		
[18]	phil			phil		38	78		
[19]	phil			phil		10^2–10^3	1–10		
[20]	phob	N	10^{-2}	phob			1–10		
[21]	phil			phil	HB		7–10		
[22]				phil	HB		1–10^2		
[23]	phob	N	10^{-1}–10	phob			3–4		
[24]	phil	HB	10–10^2	phil	HB	10–10^2			
[25]	phil		1–10^2	phil			1–10^2		
[26]	phil			phil		10^{-3}–10^{-1}			
[27]				phil	HB		10–10^3		
[28]				phil	HB		50		
[29]				phil	HB		7–10^2		

S3 Simulation rates

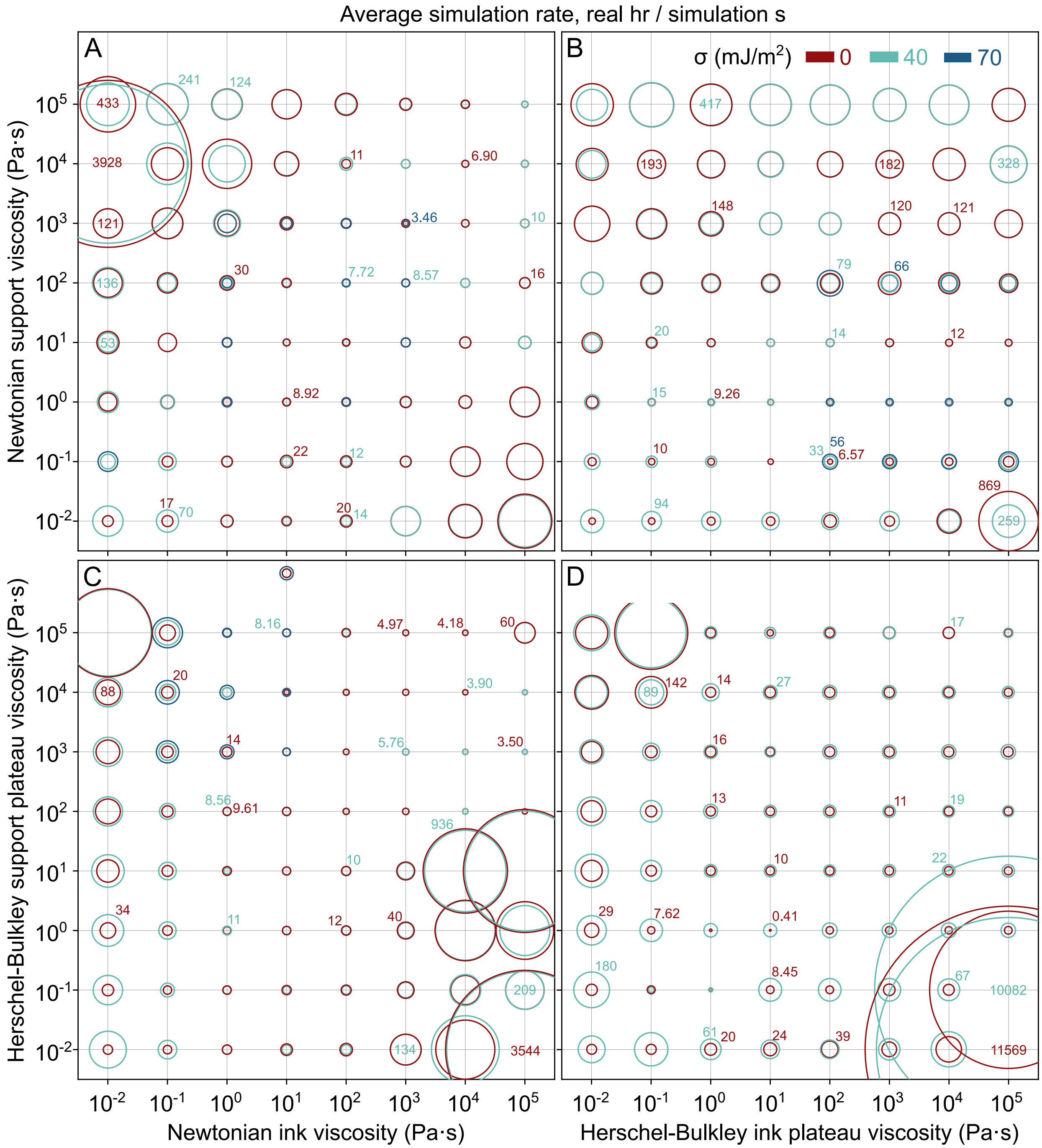

Figure S5: Simulation rates. The area of the circle represents the real time it took to run the simulation divided by the amount of time that passed within the simulation.

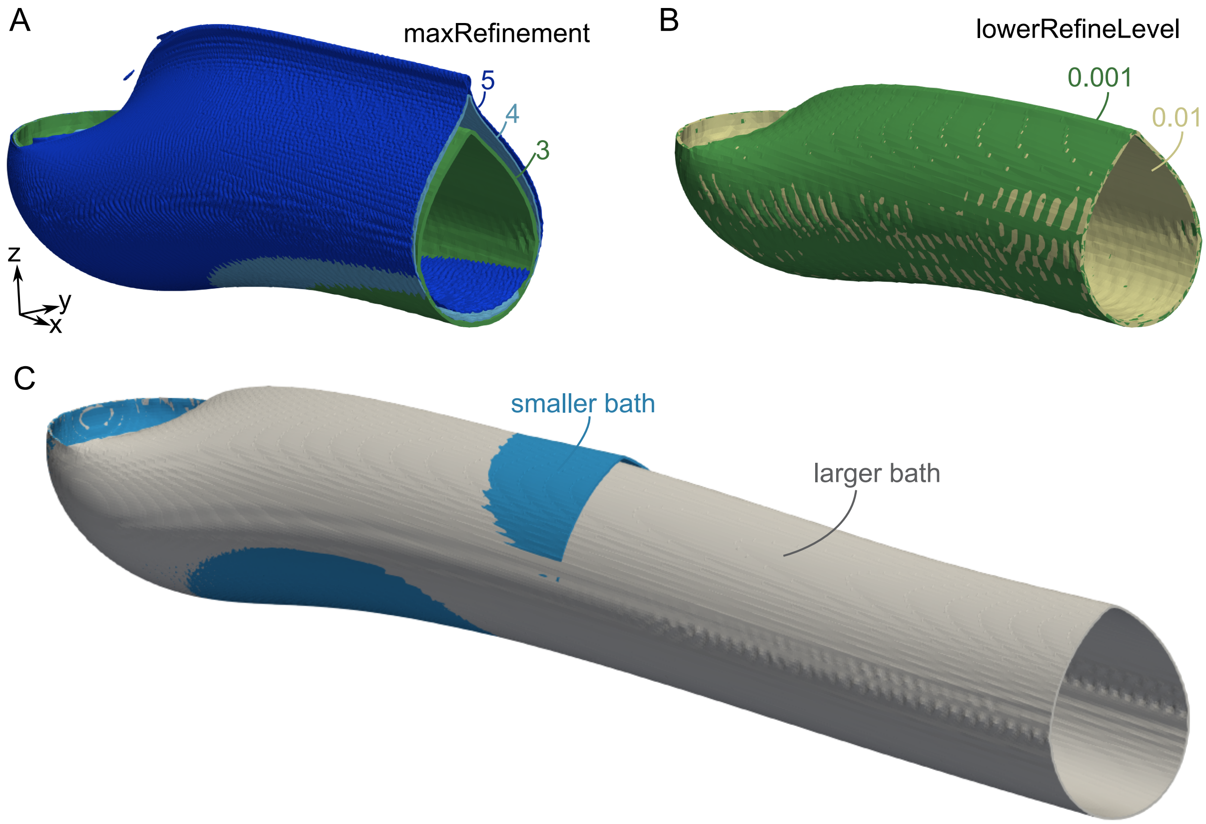

Figure S6: Mesh refinement, where both ink and support have a Newtonian viscosity of 10^3 Pa·s and the surface tension is $70\,\mathrm{mJ/m^2}$. A) A lower refinement limit of 0.001, where the mesh can be refined up to 3, 4, or 5 levels. The 4 and 5 level results are similar, but the 5 level result has slower computation times, so the lower refinement level was set to 4 for the simulations in this paper. B) Where both have a maximum remeshing level of 4, mesh refinement can occur at a volume fraction of ink below 0.999 and above 0.001 or 0.01. The limit has little effect on the result. The simulations in this paper use a limit of 0.001. C) Where all else is the same, including the initial mesh cell size, a short and long bath. The bath size has little effect. The simulations in this paper use the long bath.

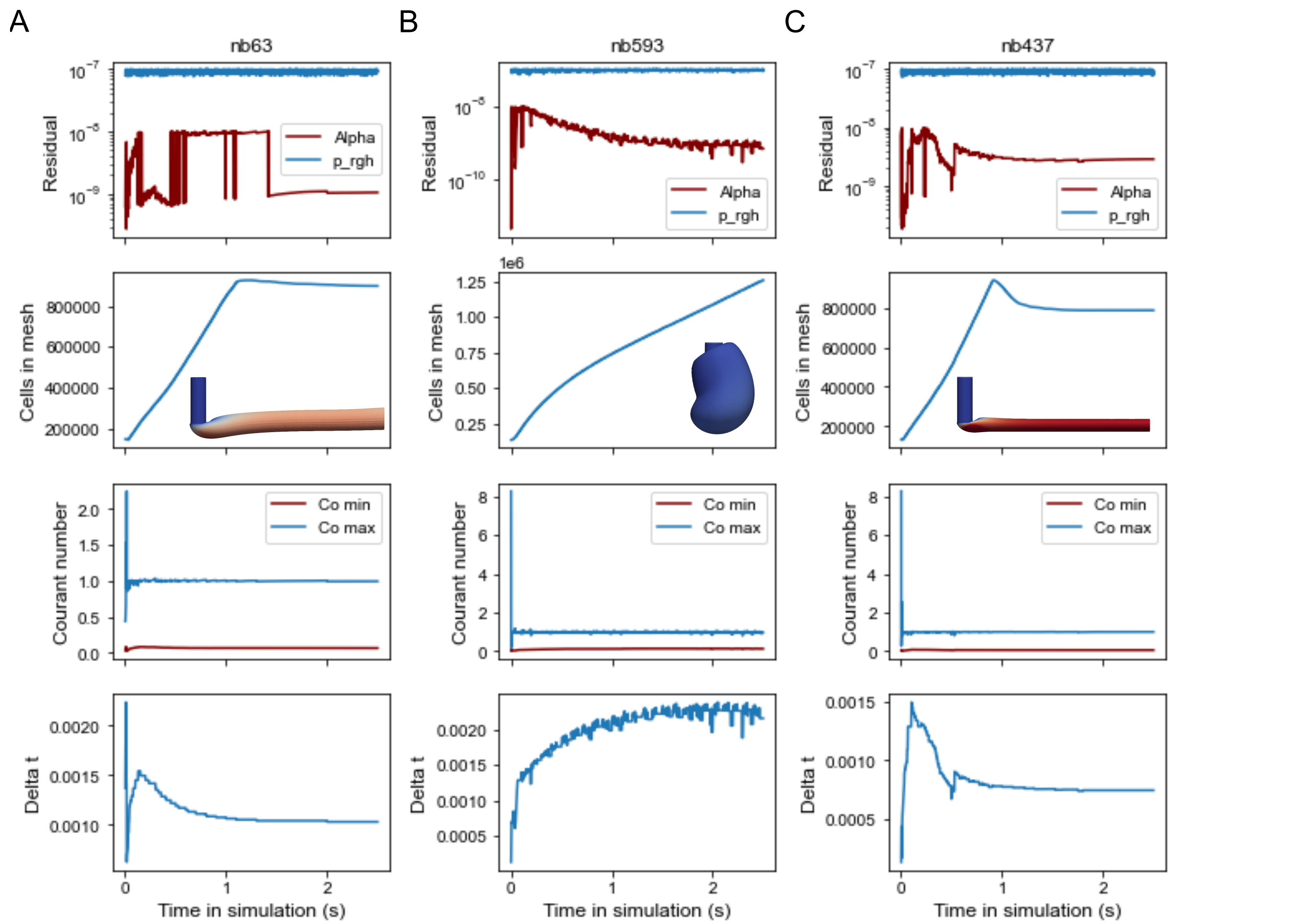

Figure S7: Convergence, where both ink and support have either a Newtonian viscosity or plateau viscosity of 10^3 Pa·s and surface tension of zero, of A) A Newtonian ink in a Newtonian support, B) A Newtonian ink in a Herschel-Bulkley support, and B) A Herschel-Bulkley ink in a Herschel-Bulkley support. Residuals for the volume fraction (alpha) and pressure (p_rgh), number of mesh cells, Courant number, and time step size plateau over the course of the simulation, unless the interface is still growing, as with the shell-like interface in B.

S4 Time series images

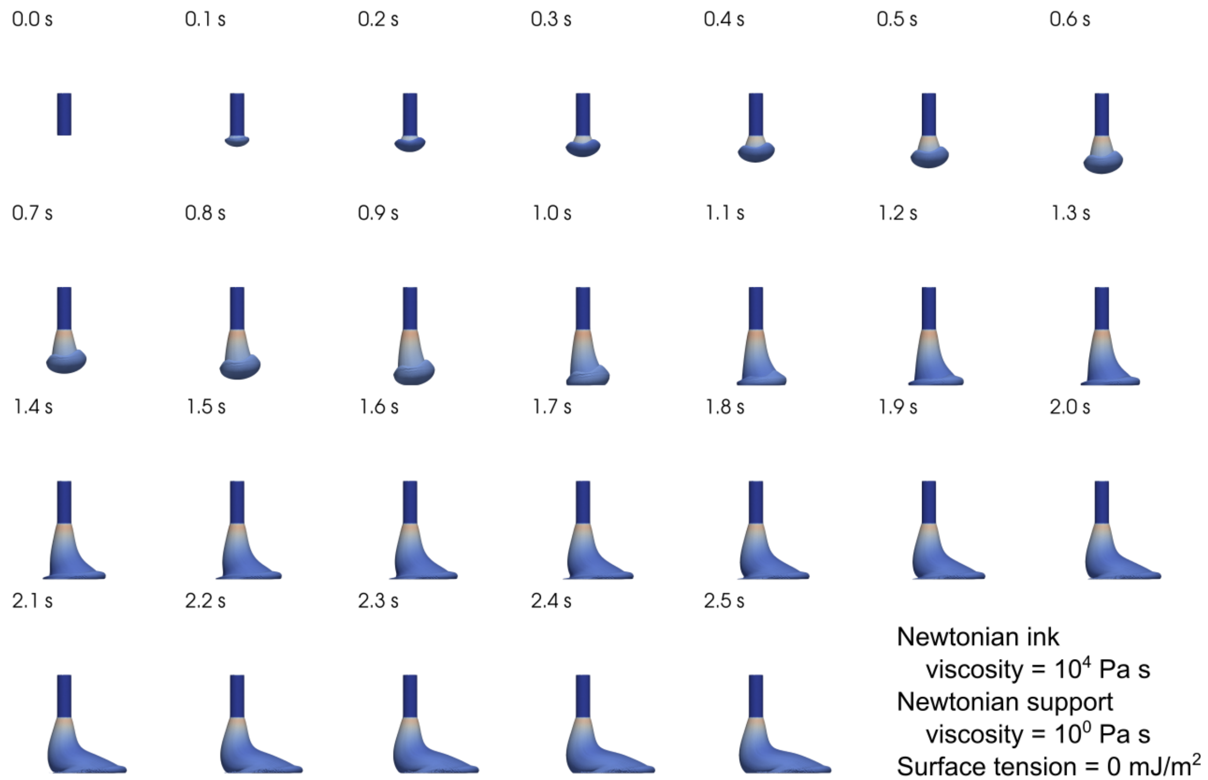

Figure S8: Extrusion of a jet at a surface tension of 0 mJ/m^2, a Newtonian support viscosity of 10^0 Pa·s, and a Newtonian ink viscosity of 10^4 Pa·s.

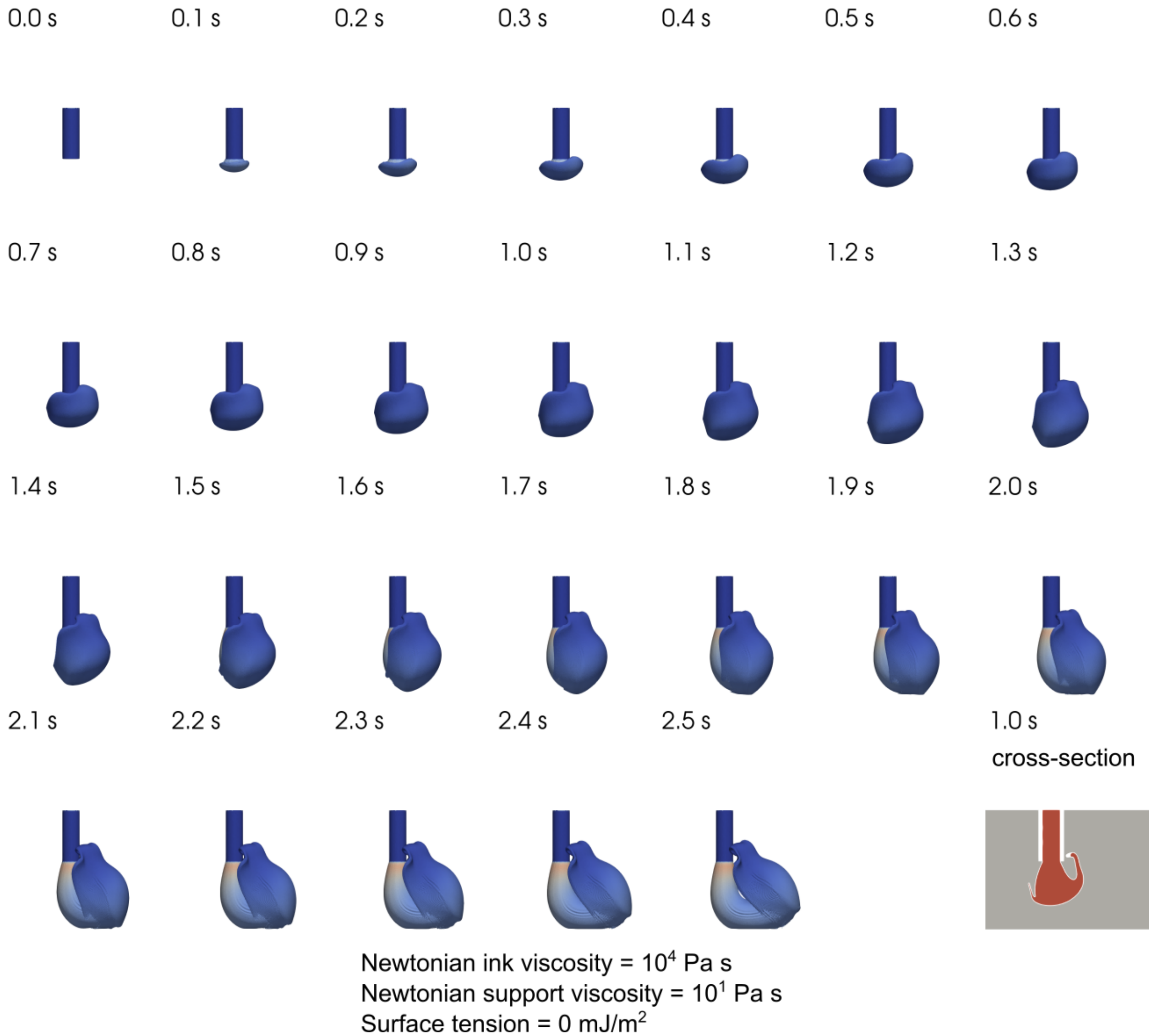

Figure S9: Extrusion of a shell at a surface tension of $0\,\mathrm{mJ/m^2}$, a Newtonian support viscosity of 10^1 Pa·s, and a Newtonian ink viscosity of 10^4 Pa·s.

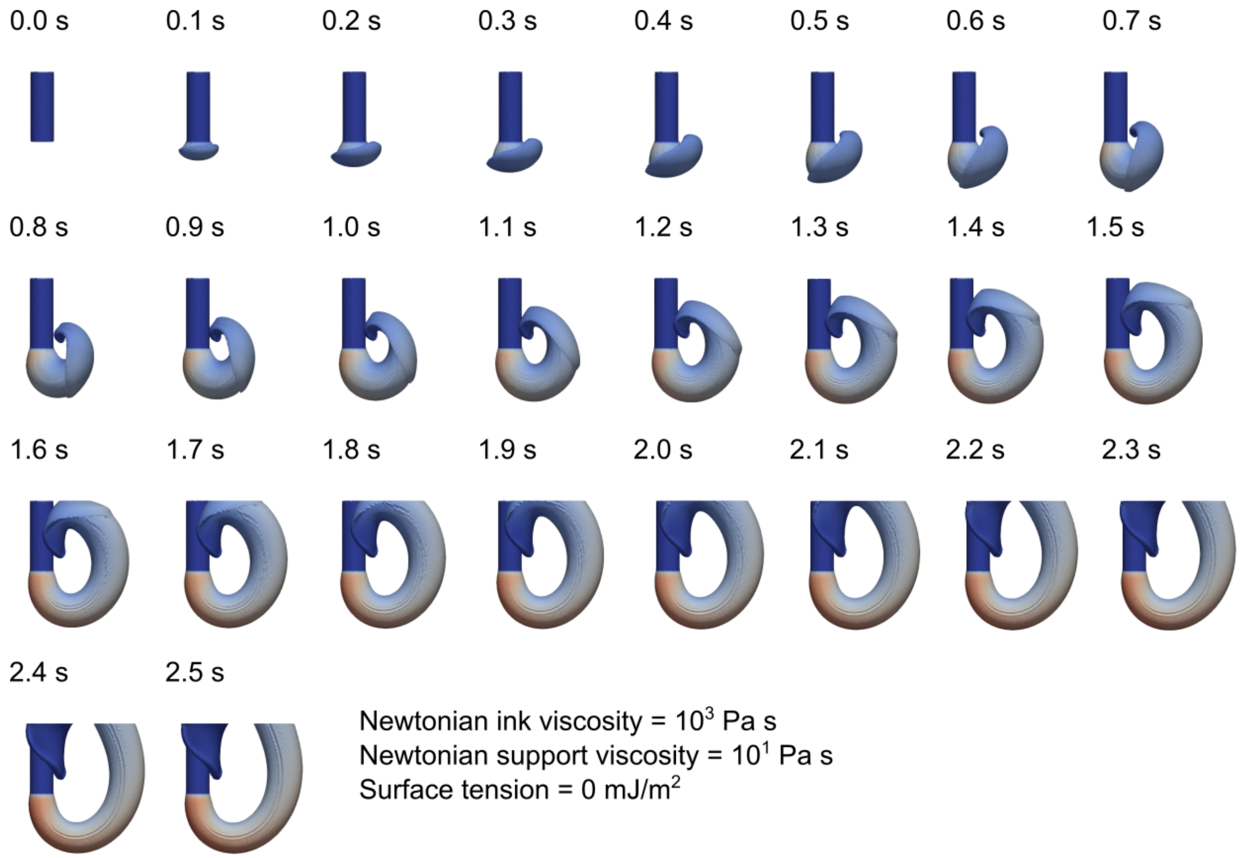

Figure S10: Extrusion of a curled filament at a surface tension of $0\,\mathrm{mJ/m^2}$, a Newtonian support viscosity of 10^1 Pa·s, and a Newtonian ink viscosity of 10^3 Pa·s.

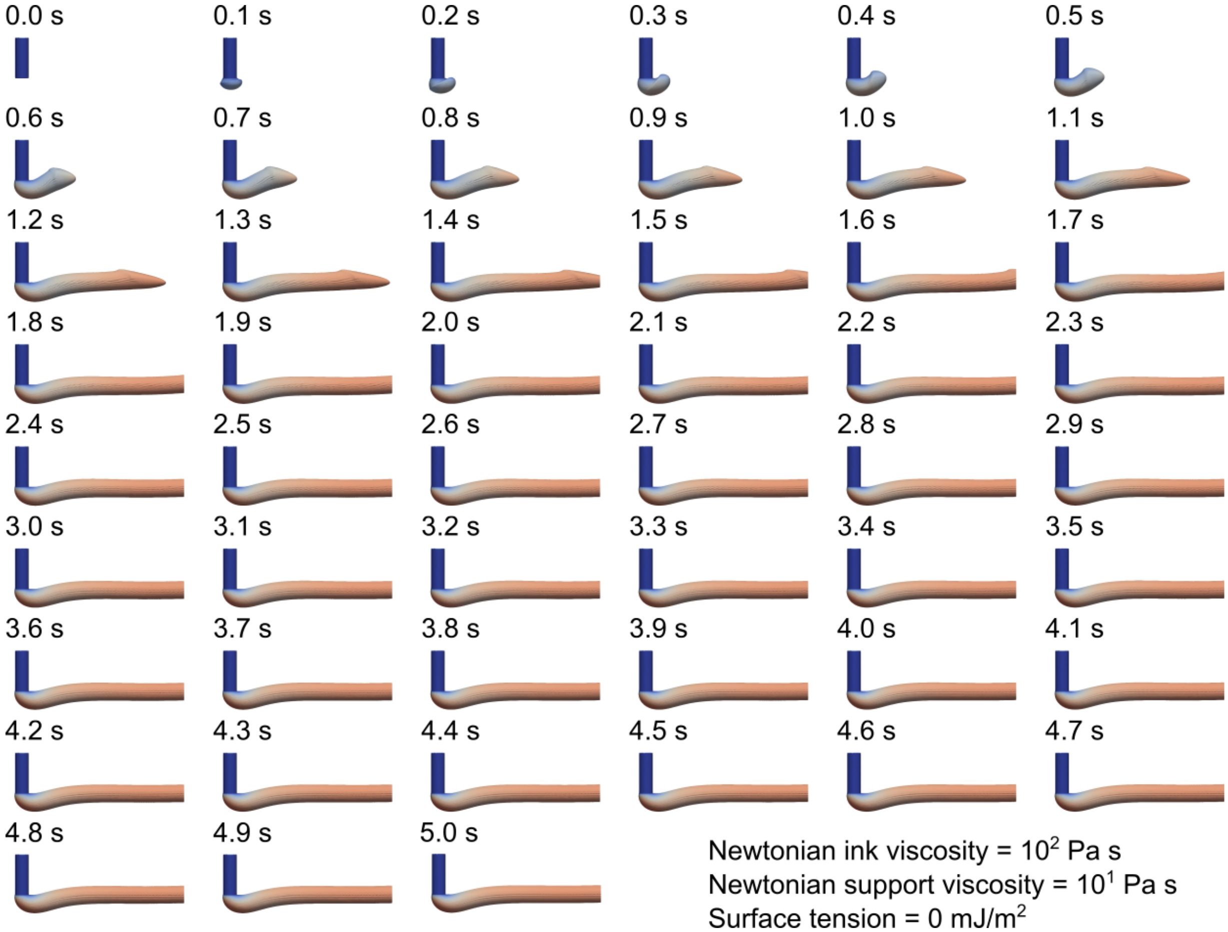

Figure S11: Extrusion of a short, fin-shaped filament at a surface tension of $0\,\mathrm{mJ/m^2}$, a Newtonian support viscosity of 10^1 Pa·s, and a Newtonian ink viscosity of 10^2 Pa·s.

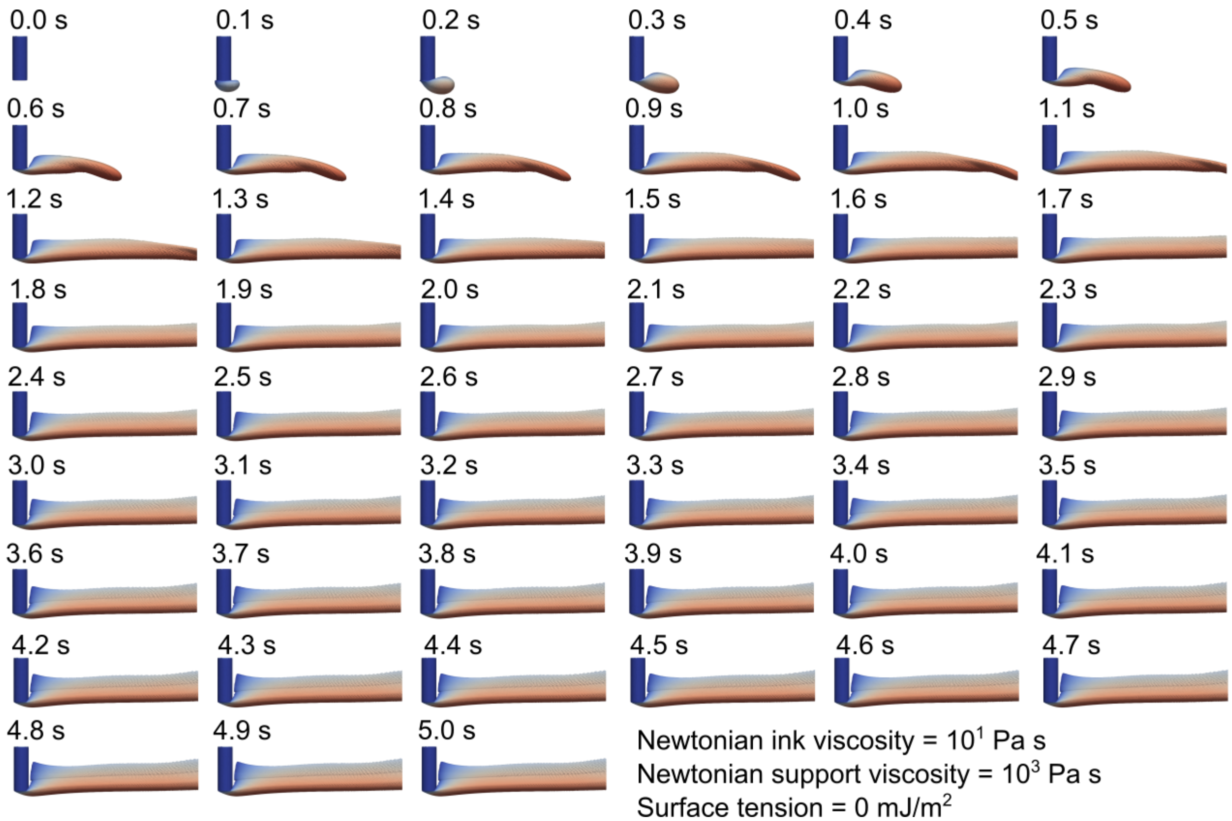

Figure S12: Extrusion of a tall, fin-shaped filament with a flat tip at a surface tension of $0\,\mathrm{mJ/m^2}$, a Newtonian support viscosity of 10^3 Pa·s, and a Newtonian ink viscosity of 10^1 Pa·s.

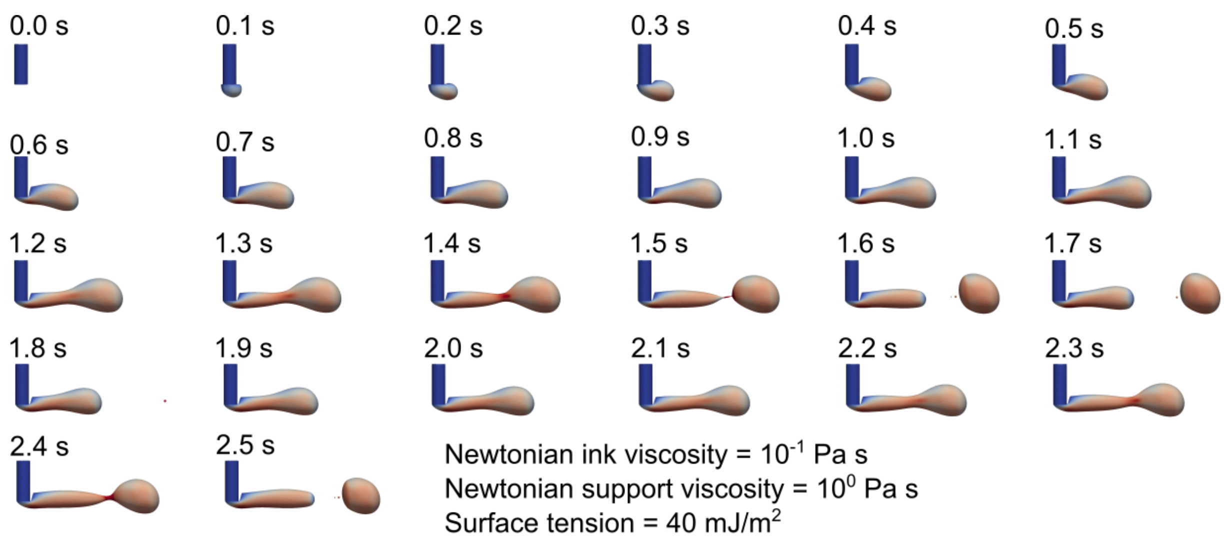

Figure S13: Breakup of a filament into droplets at a surface tension of $40\,\mathrm{mJ/m^2}$, a Newtonian support viscosity of 10^0 Pa·s, and a Newtonian ink viscosity of 10^{-1} Pa·s.

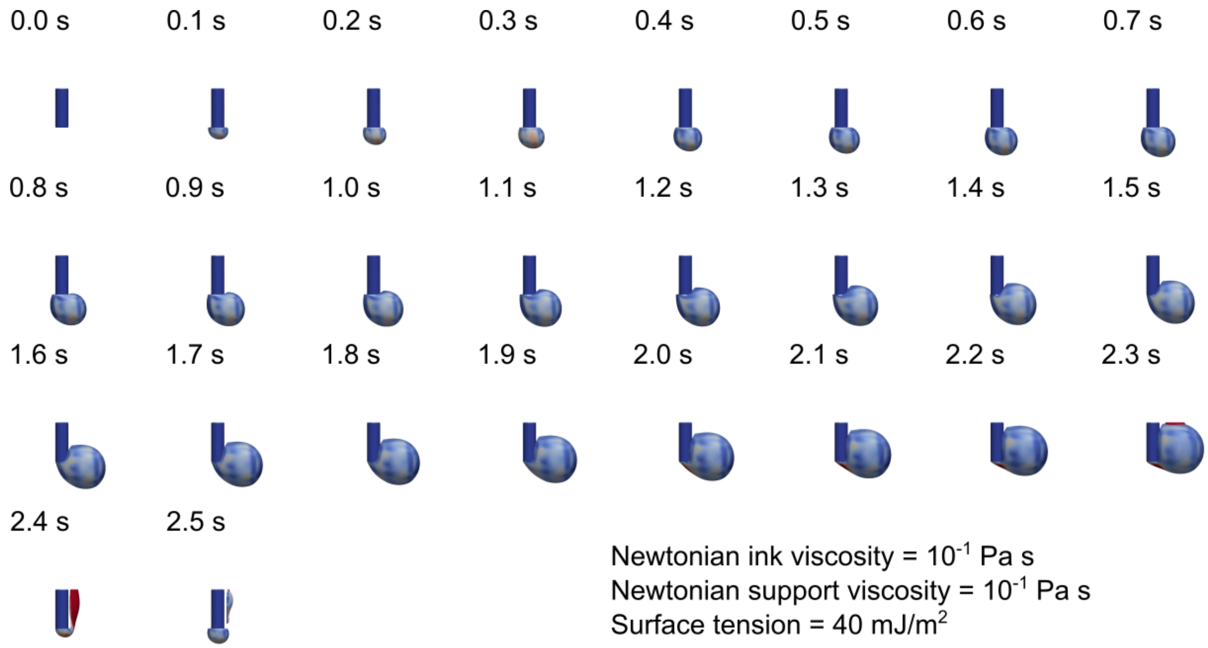

Figure S14: Breakup of a filament into droplets at a surface tension of $40\,\mathrm{mJ/m^2}$, a Newtonian support viscosity of 10^{-1} Pa·s, and a Newtonian ink viscosity of 10^{-1} Pa·s.

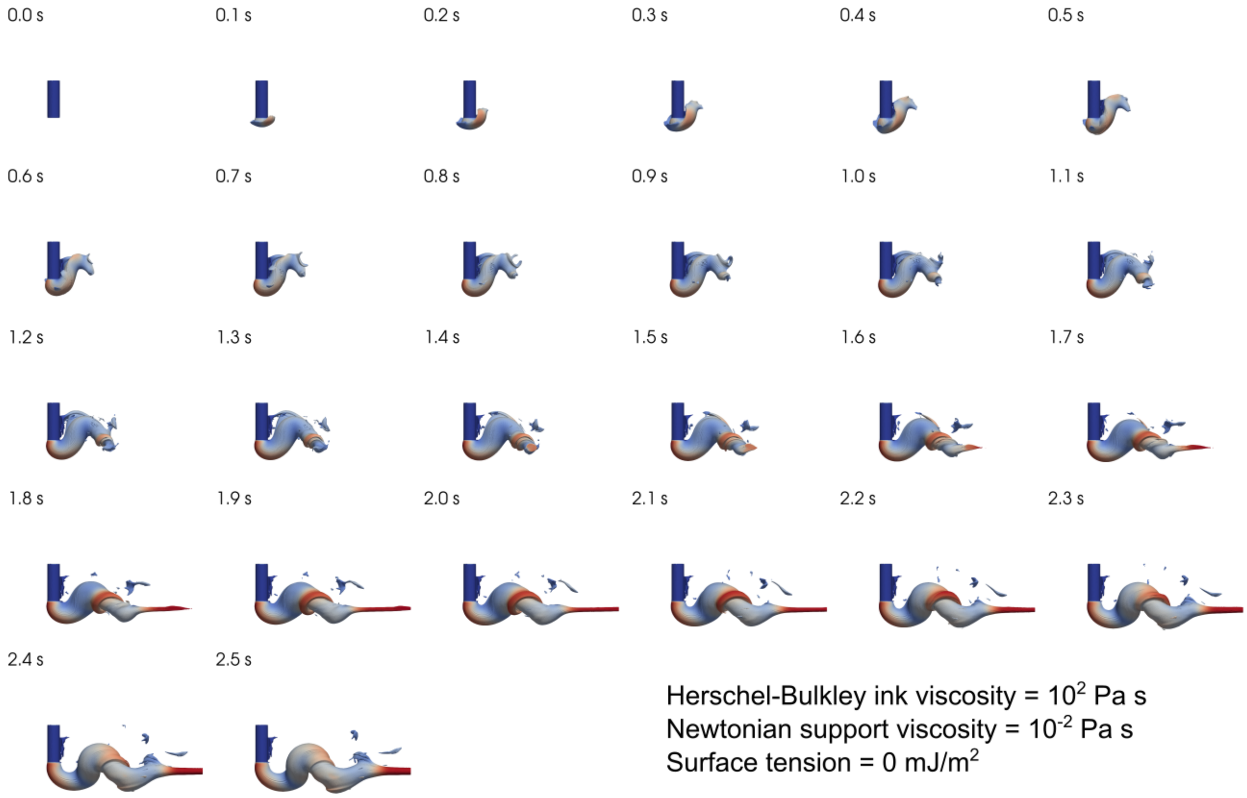

Figure S15: Extrusion of a spiraling filament at a surface tension of $0\,\mathrm{mJ/m^2}$, a Newtonian support viscosity of 10^{-2} Pa·s, and a Herschel-Bulkley ink viscosity of 10^2 Pa·s.

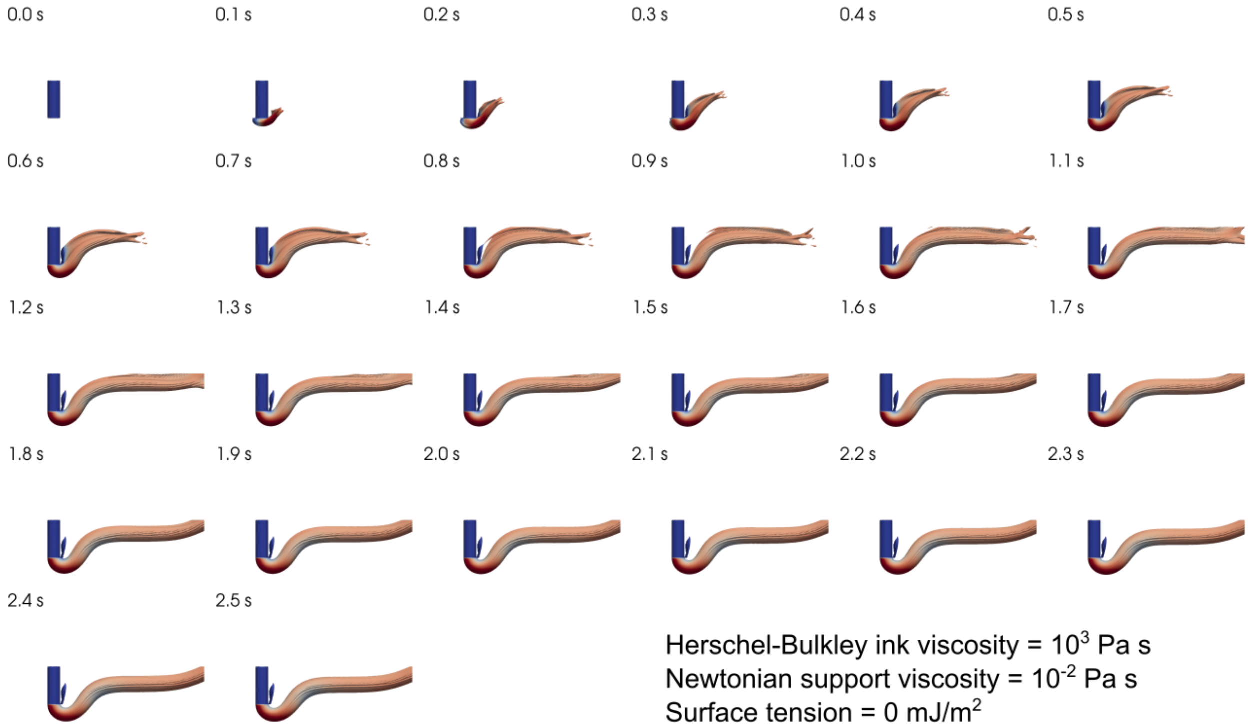

Figure S16: Extrusion of a vertically distorted, splashing filament at a surface tension of $0\,\mathrm{mJ/m^2}$, a Newtonian support viscosity of 10^{-2} Pa·s, and a Herschel-Bulkley ink viscosity of 10^3 Pa·s.

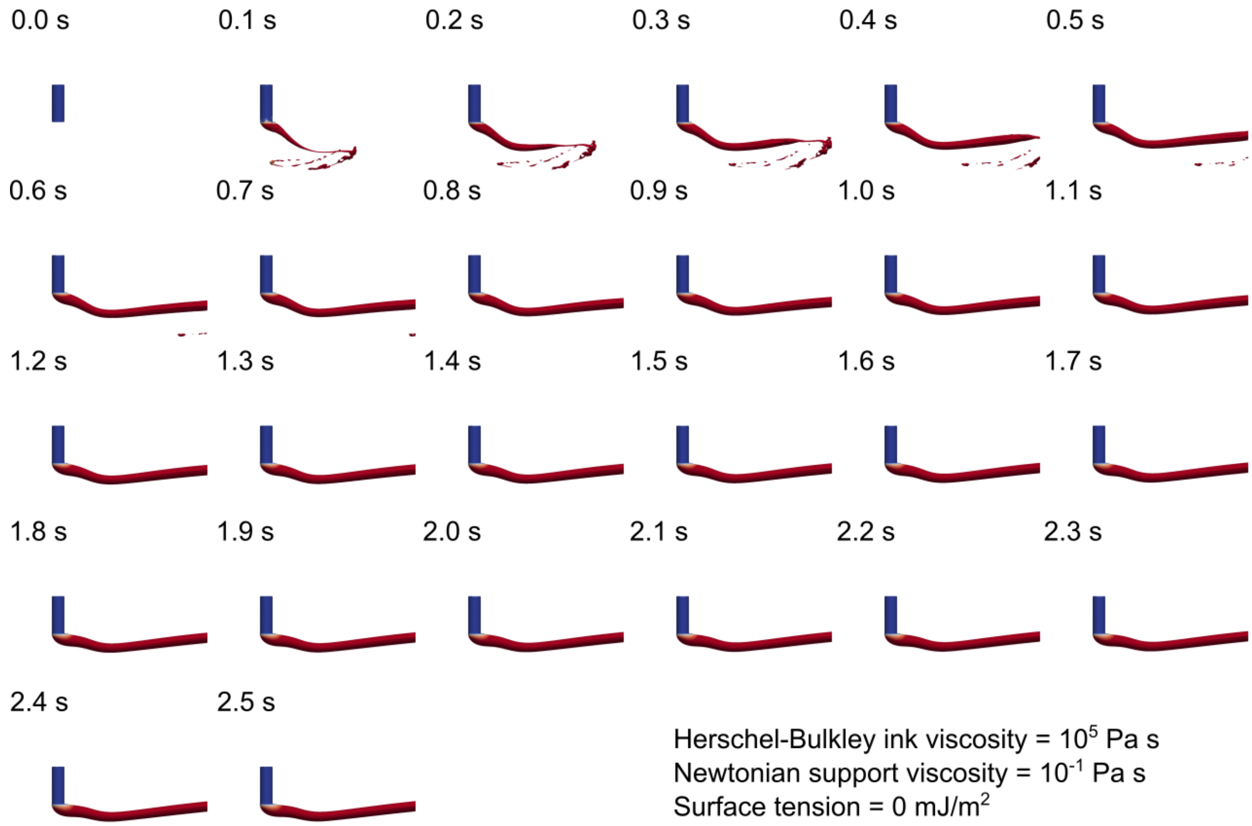

Figure S17: Extrusion of a distorted, splattering filament at a surface tension of $0\,\mathrm{mJ/m^2}$, a Newtonian support viscosity of 10^0 Pa·s, and a Herschel-Bulkley ink viscosity of 10^4 Pa·s.

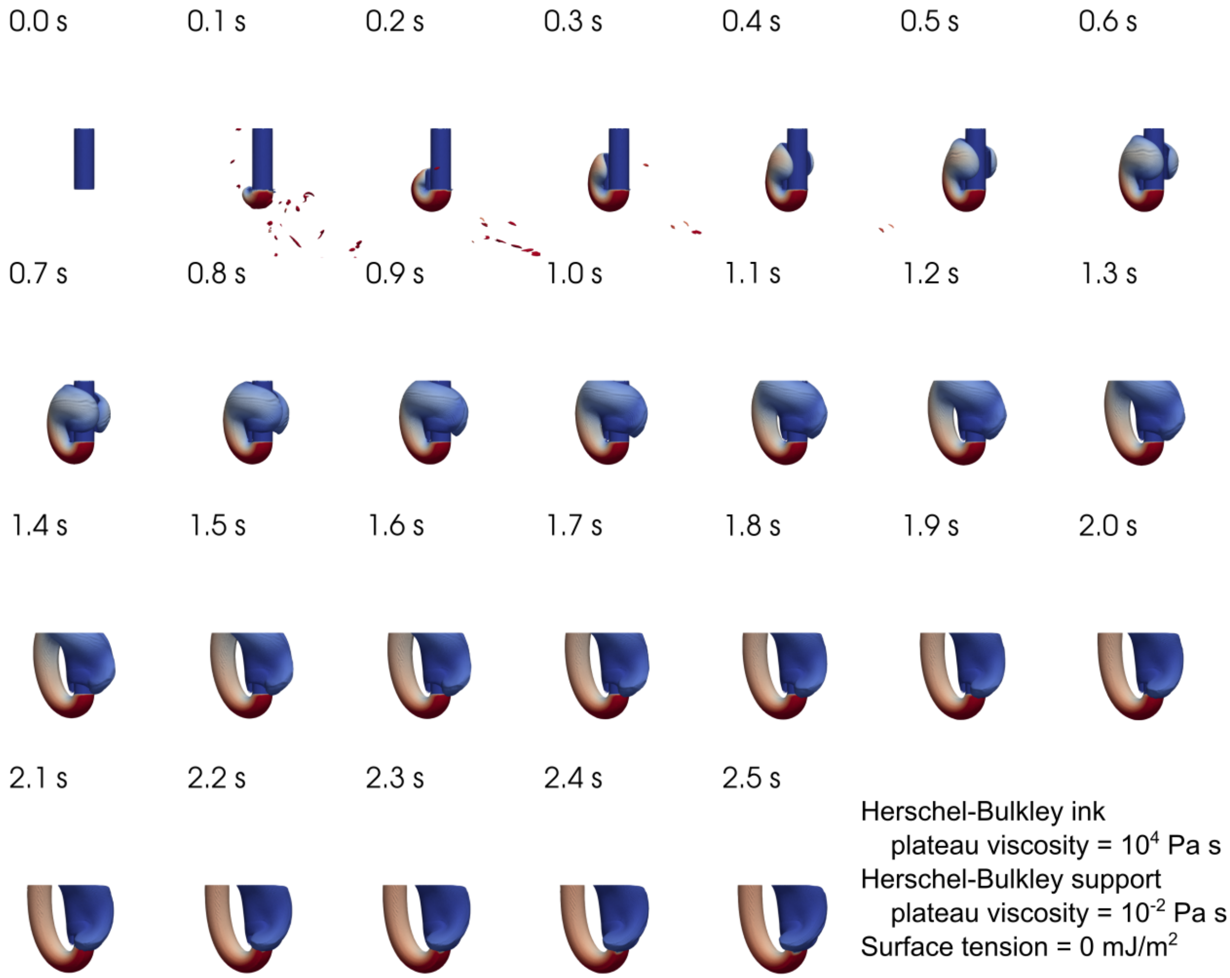

Figure S18: Extrusion of a curled filament at $\sigma = 0$ mJ/m^2, a Herschel-Bulkley support plateau viscosity of 10^{-2} Pa·s, and a Herschel-Bulkley ink plateau viscosity of 10^4 Pa·s.

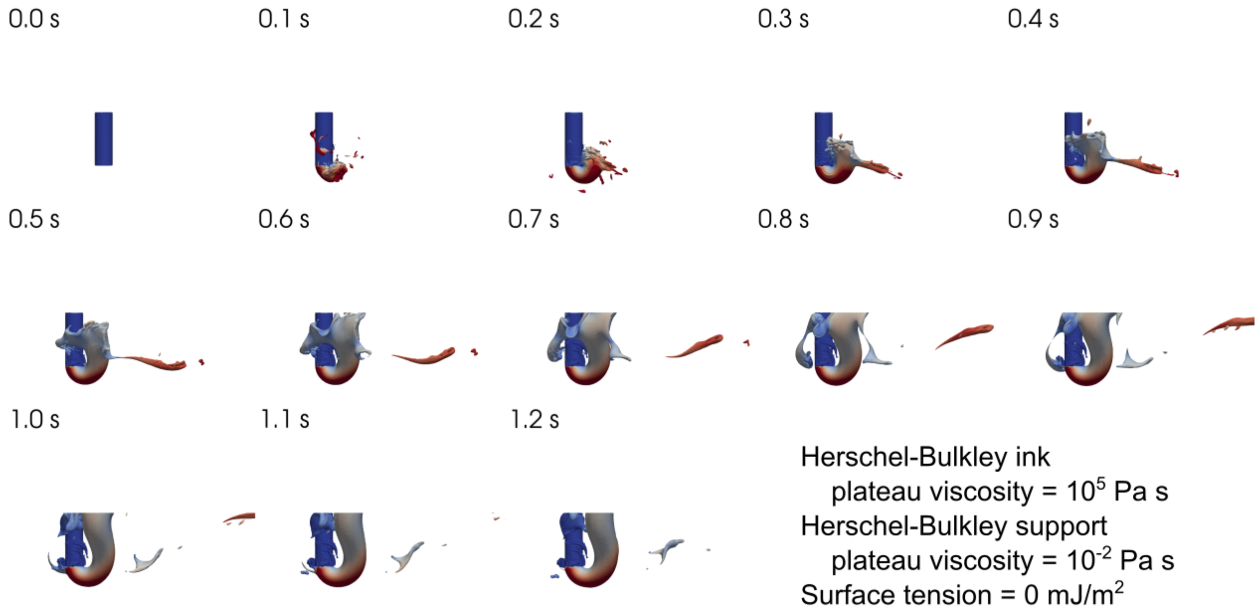

Figure S19: Extrusion of a curled filament at a surface tension of $0\,\mathrm{mJ/m^2}$, a Herschel-Bulkley support plateau viscosity of 10^{-2} Pa·s, and a Herschel-Bulkley ink plateau viscosity of 10^4 Pa·s.

S5 Quantifying cross-sections

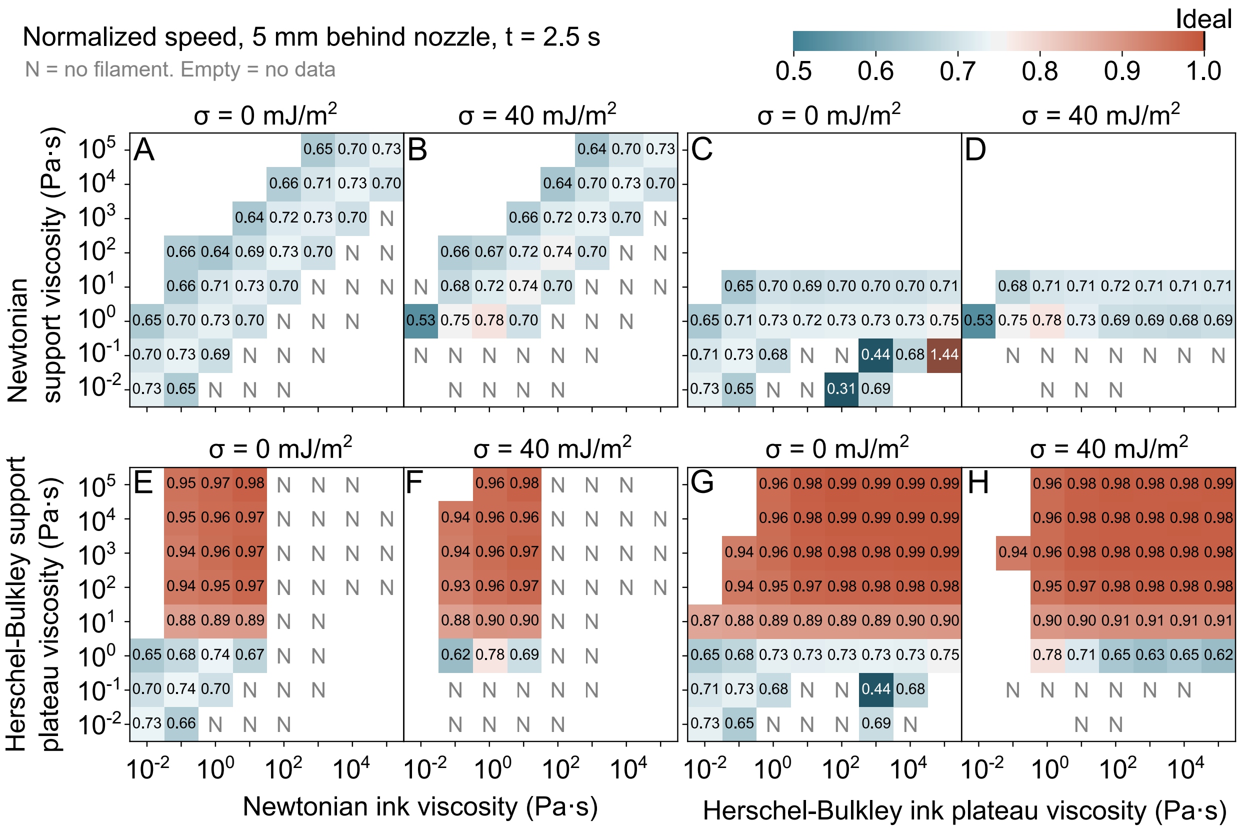

Figure S20: Average speed, normalized by the intended speed of 10 mm/s, within filament cross-sections, collected 5 mm downstream of the nozzle after 2.5 s of flow.

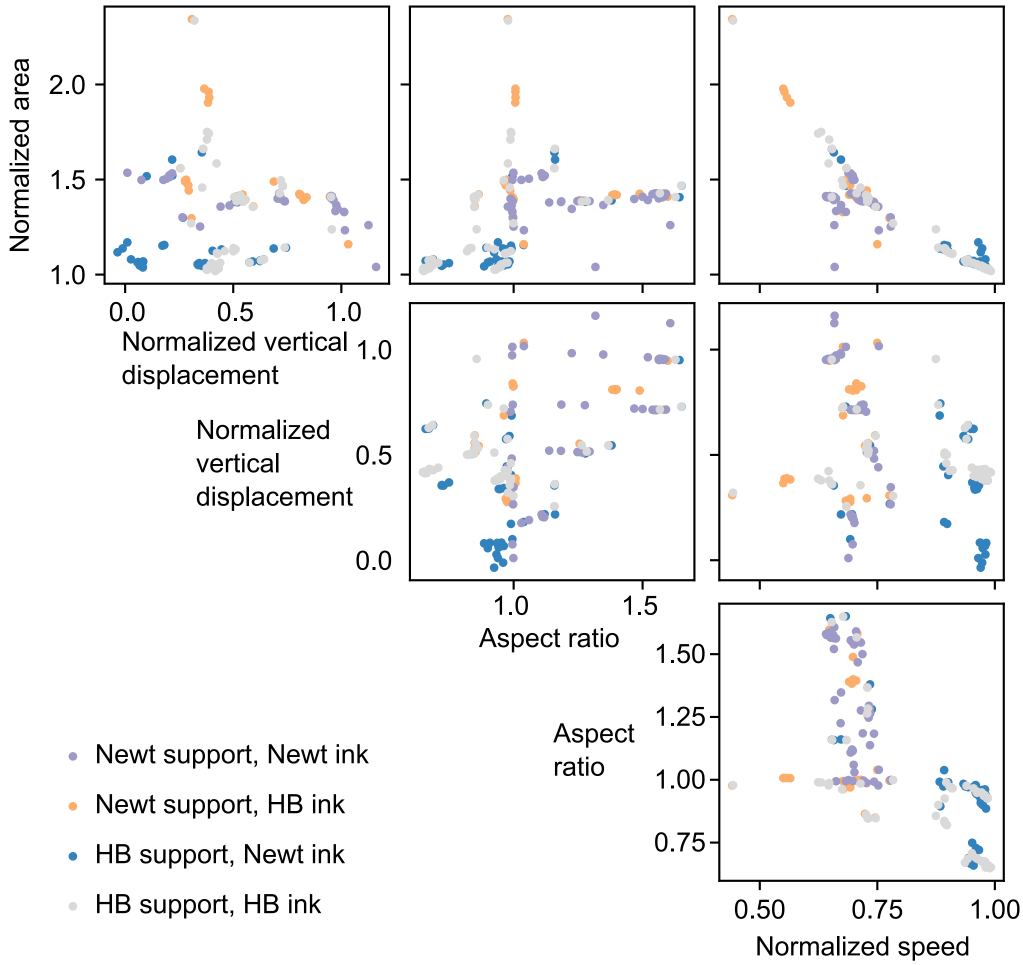

Figure S21: Correlations between filament cross-section metrics. The normalized speed is the average flow velocity in the filament divided by the bath translation speed (10 mm/s). The vertical displacement is the distance between the bottom of the filament and the intended position of the bottom of the filament, divided by the nozzle inner diameter. The area is the cross-sectional area divided by the inner area of the nozzle. The aspect ratio is the maximum height of the filament divided by the maximum width.

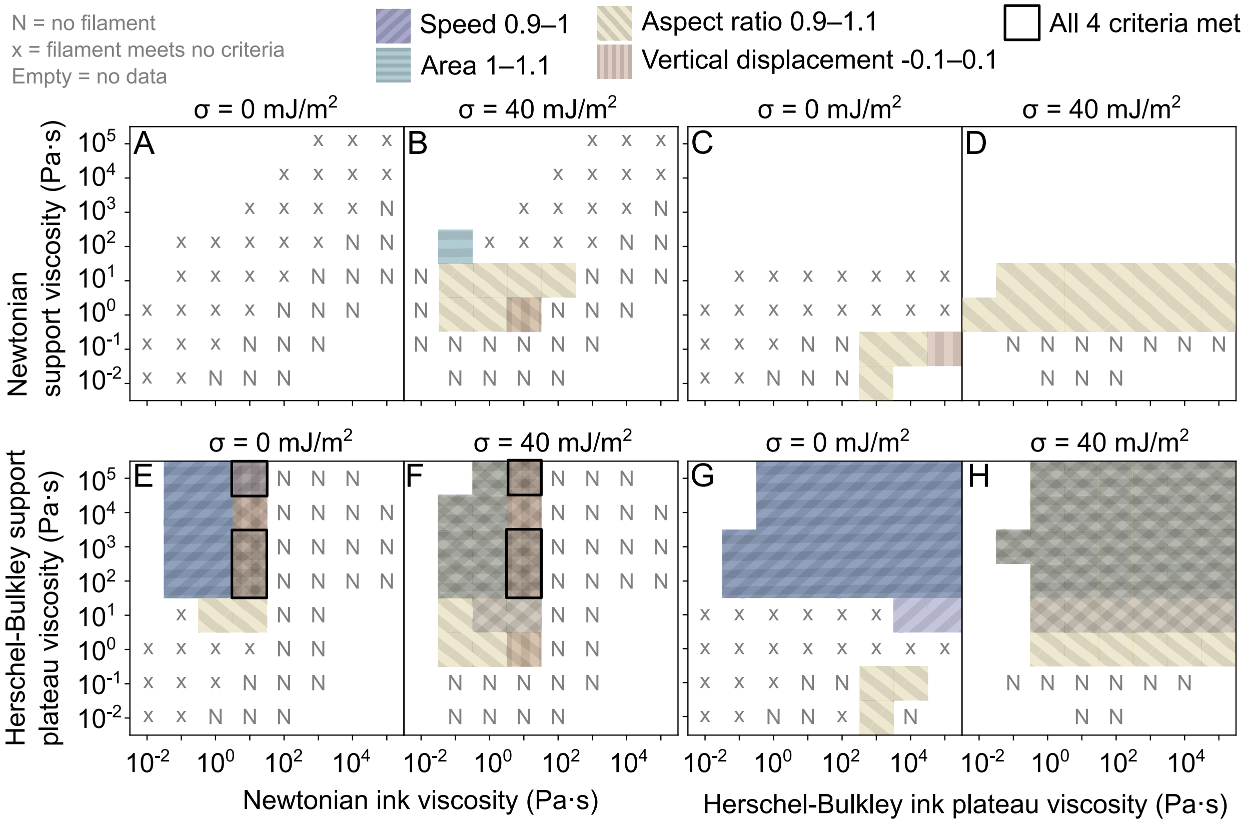

Figure S22: Summary of quantitative cross-section measurements. Simulations where the four listed metrics are close to ideal are framed in black.

S6 Filament stability

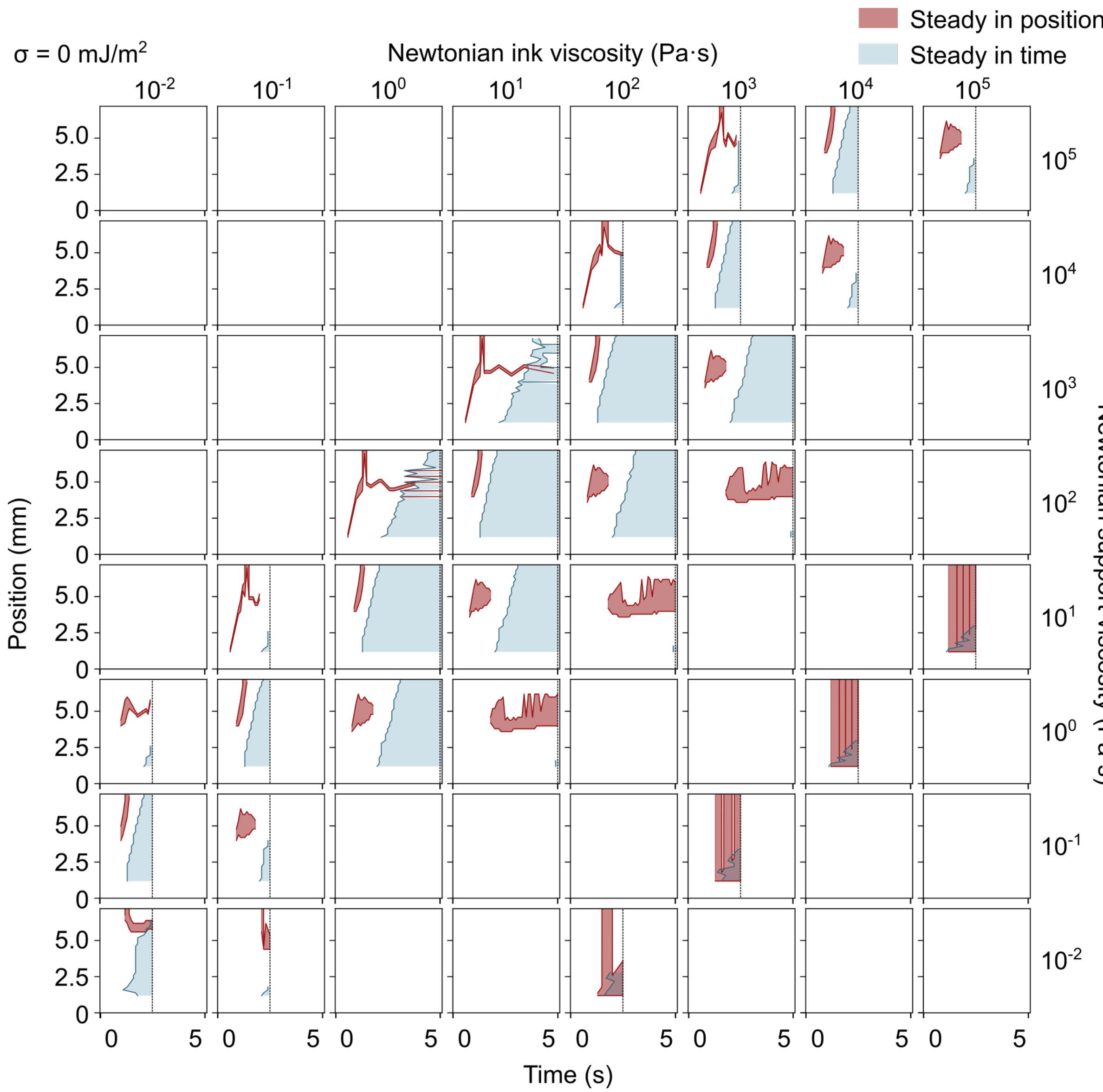

Figure S23: Stability metrics at a surface tension of $0\,\mathrm{mJ/m^2}$, where the ink and support are both Newtonian. Stability is defined here using the position of the bottom of the filament. Steady in position means that at a given time, the filament cross-section doesn't change within the plotted span in position. Steady in time means that at a given position, the filament cross-section doesn't change over the plotted span in time.

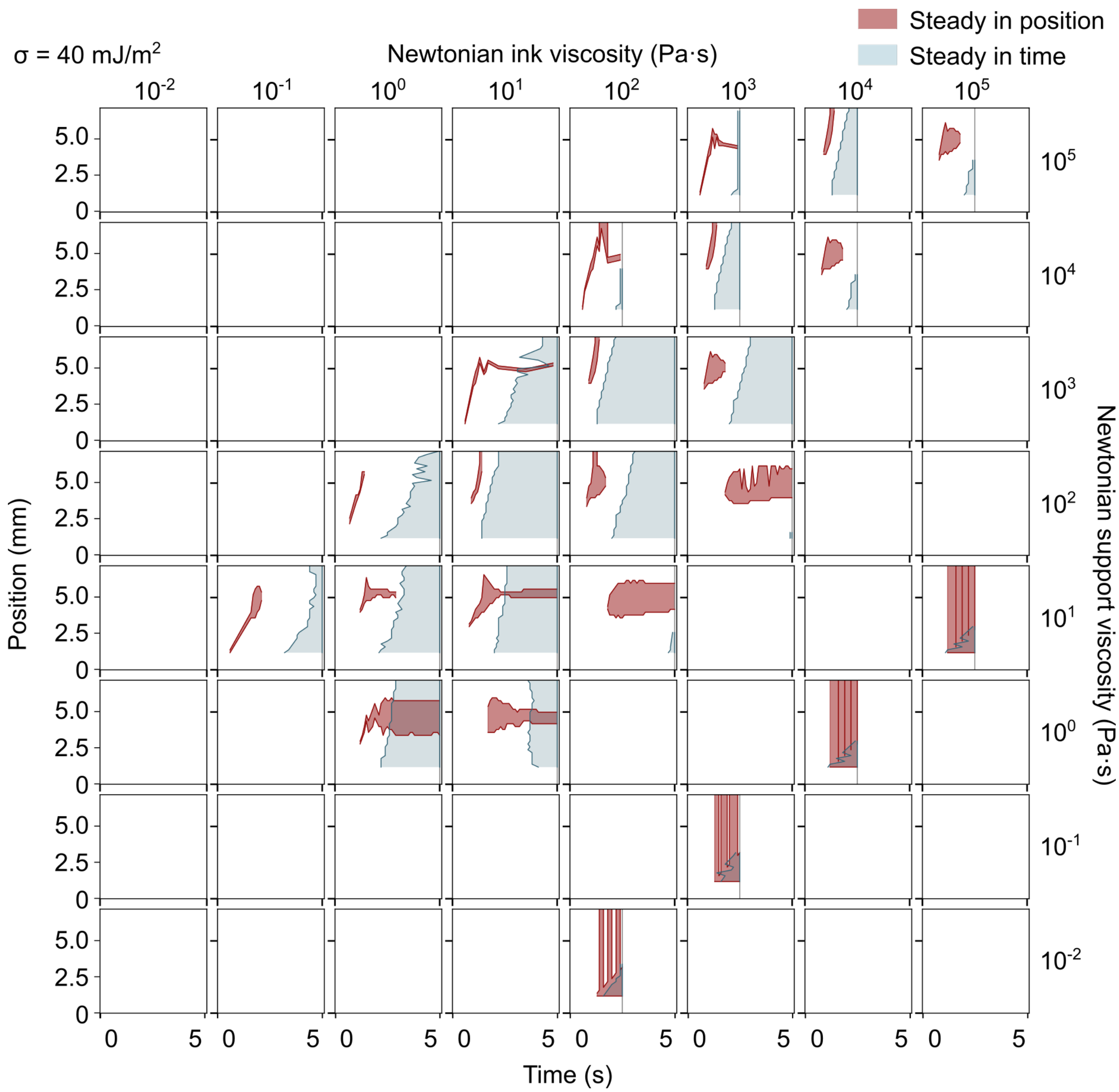

Figure S24: Stability metrics at a surface tension of $40\,\mathrm{mJ/m^2}$, where the ink and support are both Newtonian. Stability is defined here using the position of the bottom of the filament. Steady in position means that at a given time, the filament cross-section doesn't change within the plotted span in position. Steady in time means that at a given position, the filament cross-section doesn't change over the plotted span in time.

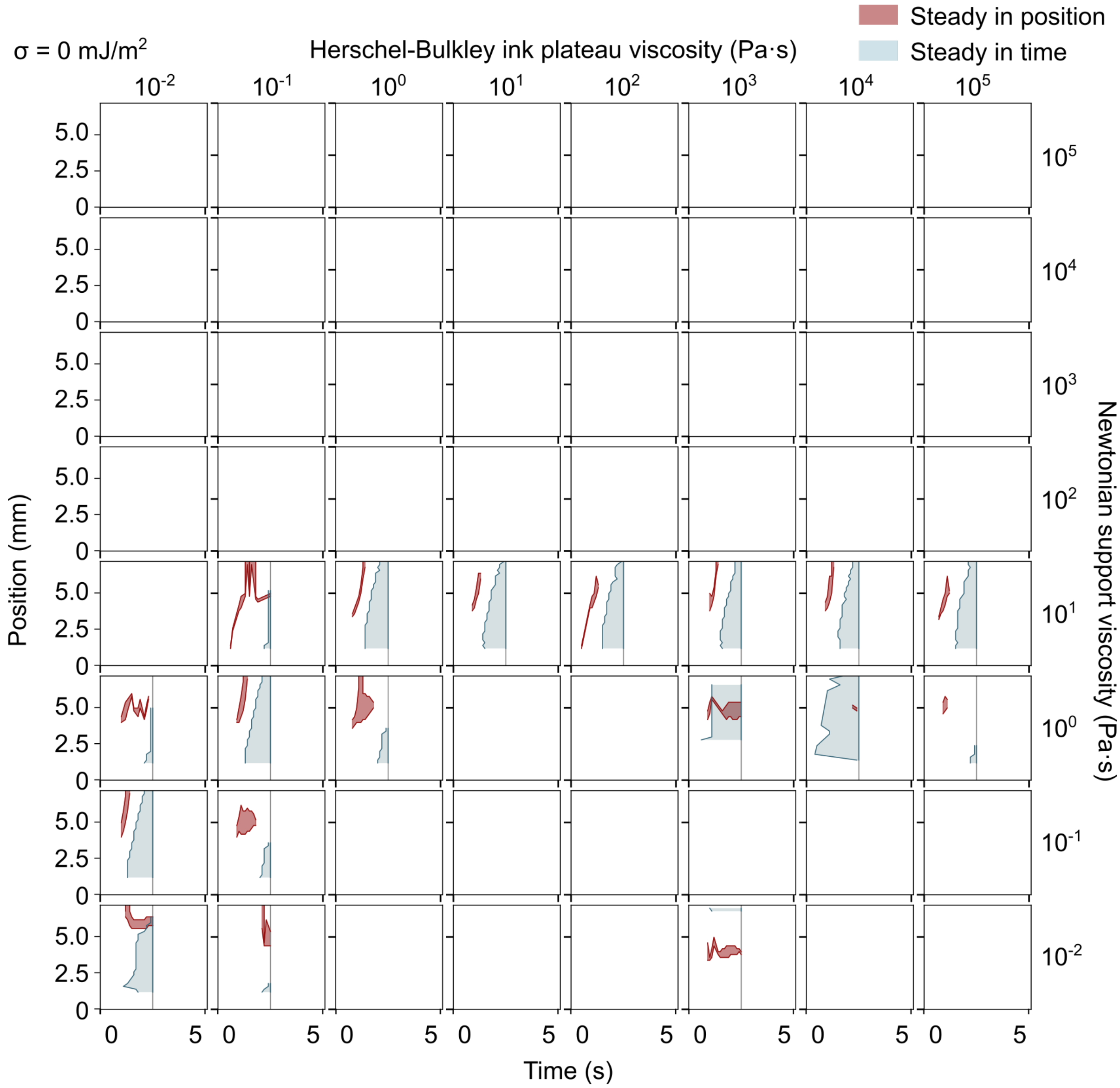

Figure S25: Stability metrics at a surface tension of $0\,\mathrm{mJ/m^2}$, where the ink is a Herschel-Bulkley fluid and the support is Newtonian. Stability is defined here using the position of the bottom of the filament. Steady in position means that at a given time, the filament cross-section doesn't change within the plotted span in position. Steady in time means that at a given position, the filament cross-section doesn't change over the plotted span in time.

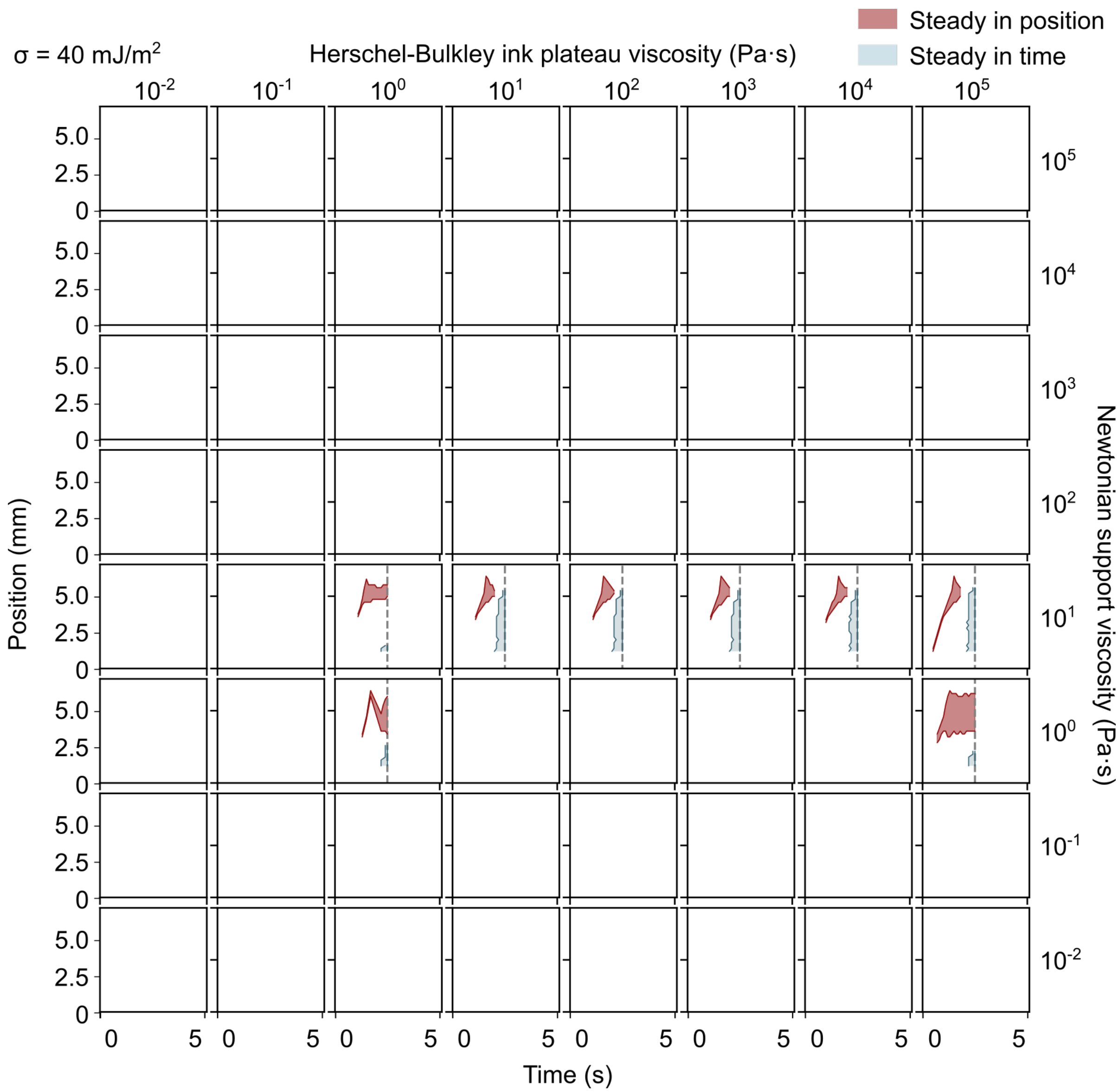

Figure S26: Stability metrics at a surface tension of $40\,\mathrm{mJ/m^2}$, where the ink is a Herschel-Bulkley fluid and the support is Newtonian. Stability is defined here using the position of the bottom of the filament. Steady in position means that at a given time, the filament cross-section doesn't change within the plotted span in position. Steady in time means that at a given position, the filament cross-section doesn't change over the plotted span in time.

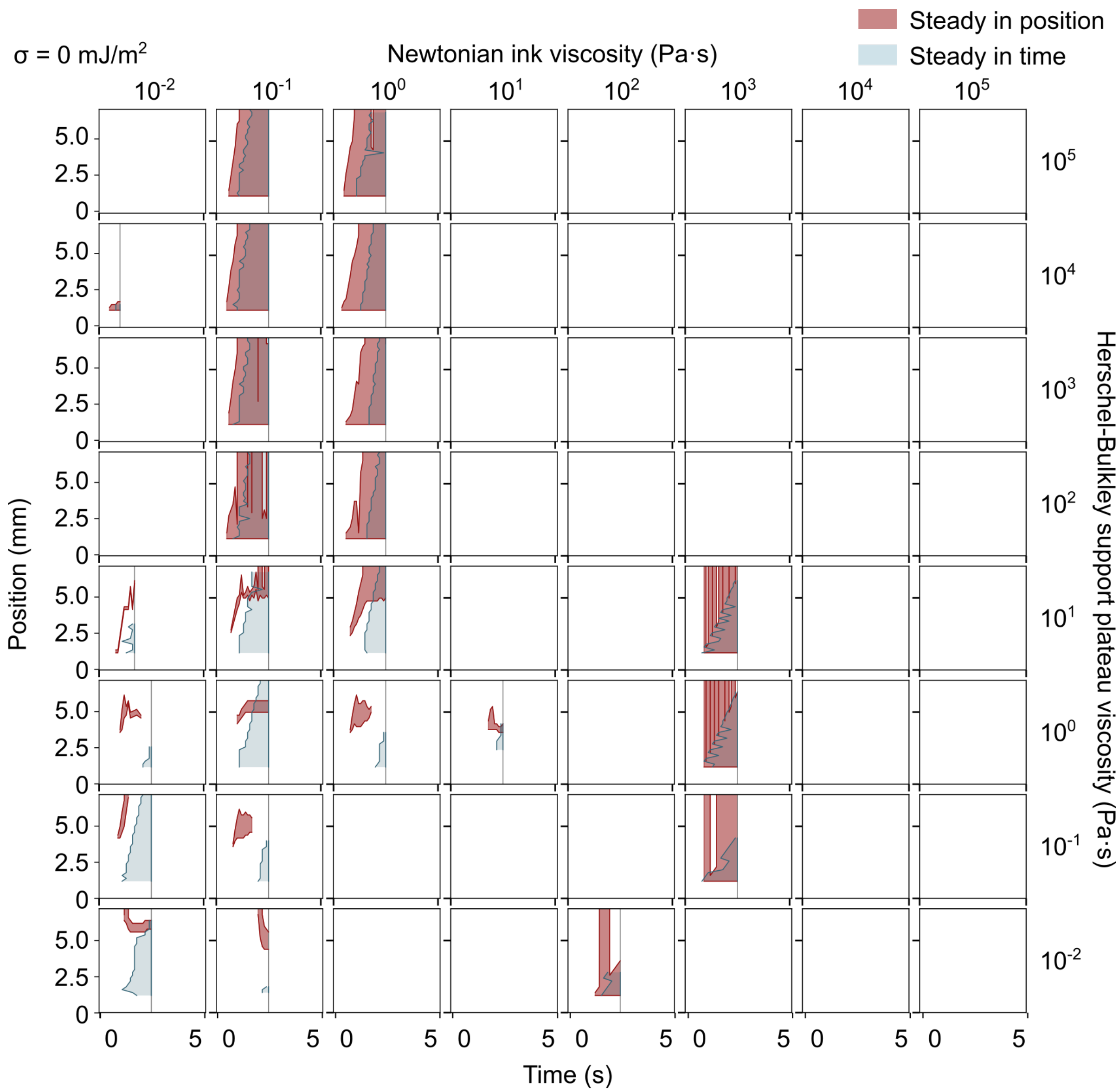

Figure S27: Stability metrics at a surface tension of $0\,\mathrm{mJ/m^2}$, where the ink is Newtonian and the support is a Herschel-Bulkley fluid. Stability is defined here using the position of the bottom of the filament. Steady in position means that at a given time, the filament cross-section doesn't change within the plotted span in position. Steady in time means that at a given position, the filament cross-section doesn't change over the plotted span in time.

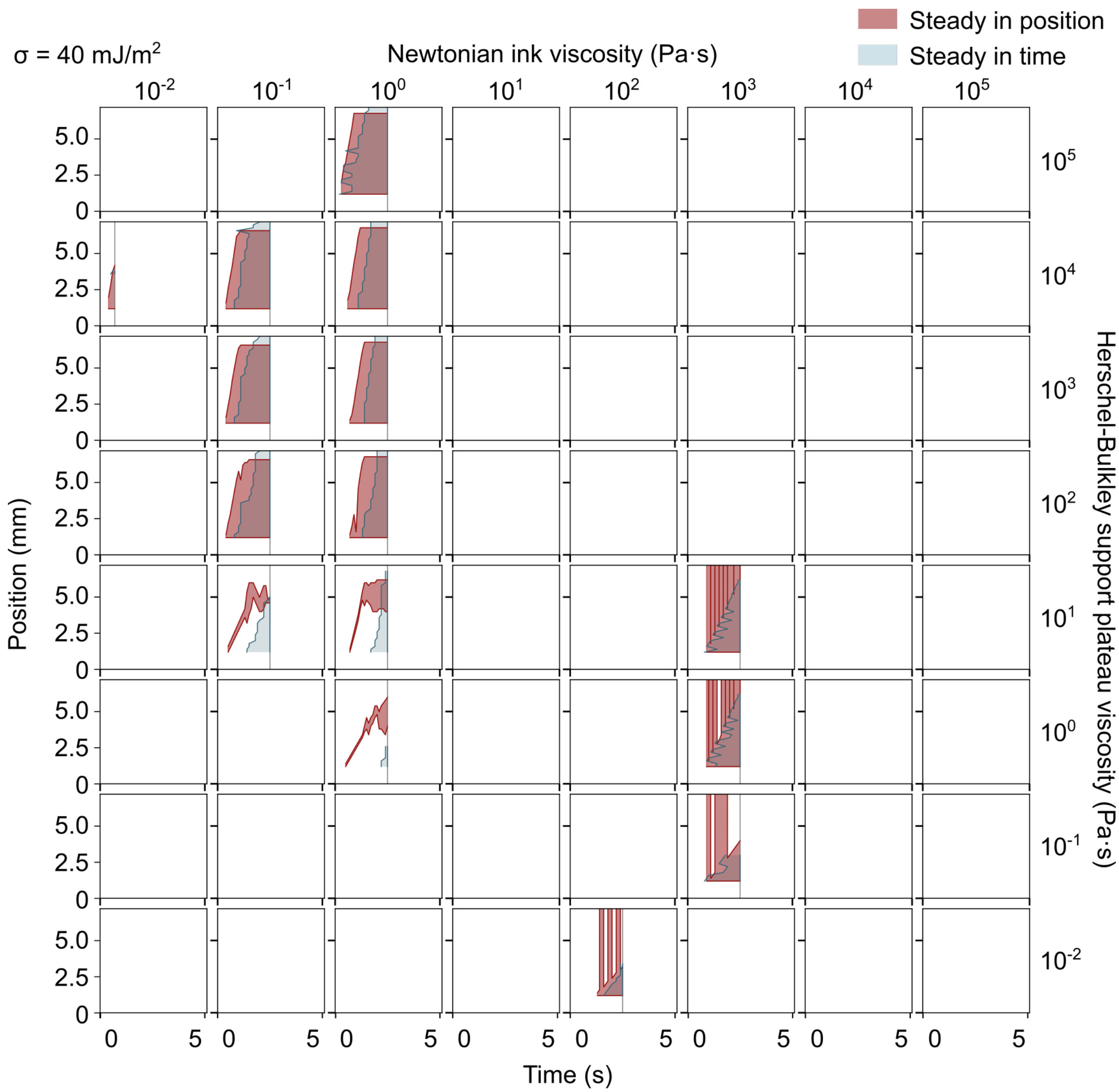

Figure S28: Stability metrics at $\sigma = 40$ mJ/m^2, where the ink is Newtonian and the support is a Herschel-Bulkley fluid. Stability is defined here using the position of the bottom of the filament. Steady in position means that at a given time, the filament cross-section doesn't change within the plotted span in position. Steady in time means that at a given position, the filament cross-section doesn't change over the plotted span in time.

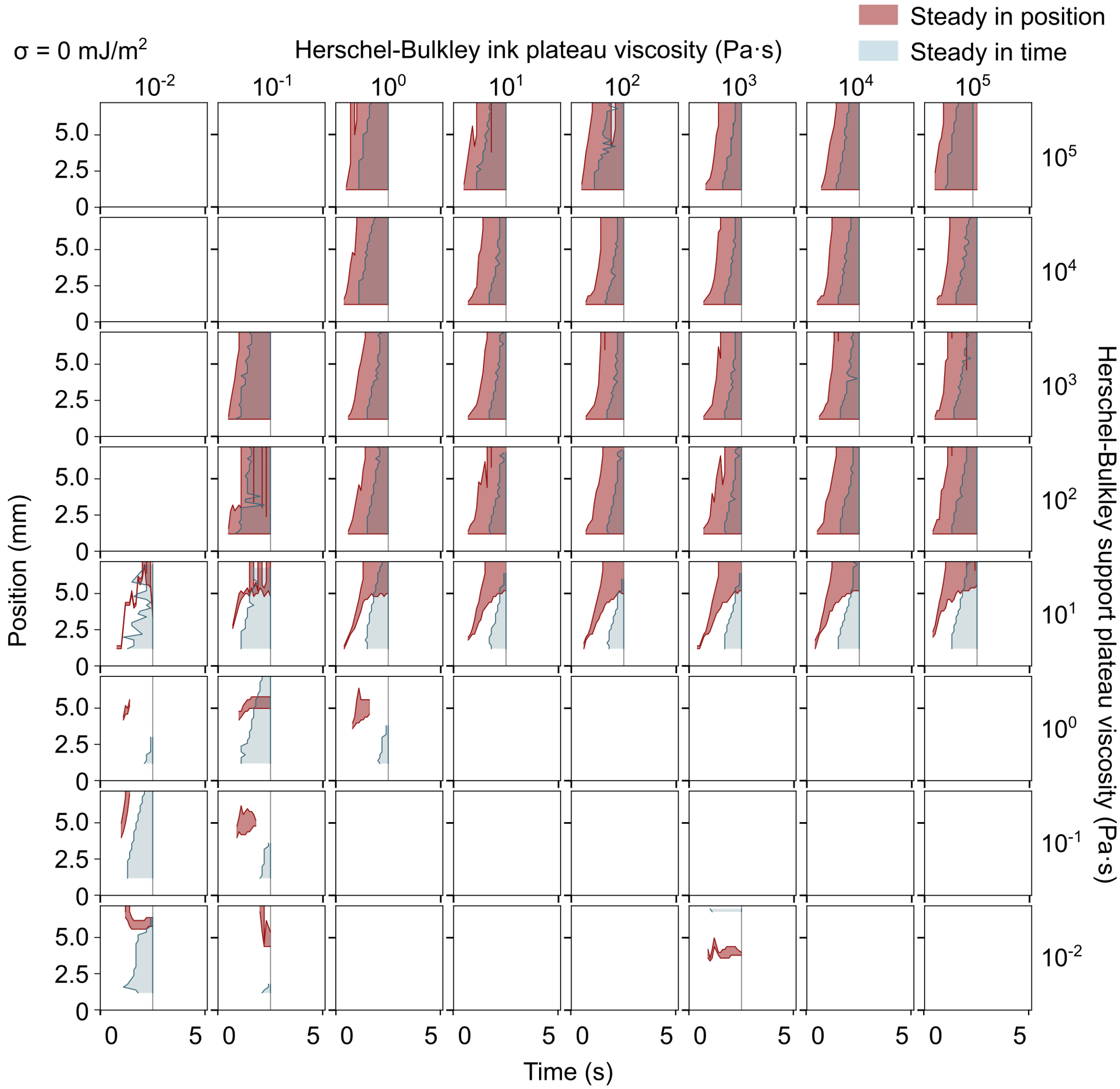

Figure S29: Stability metrics at a surface tension of $0\,\mathrm{mJ/m^2}$, where the ink and support are both Herschel-Bulkley fluids. Stability is defined here using the position of the bottom of the filament. Steady in position means that at a given time, the filament cross-section doesn't change within the plotted span in position. Steady in time means that at a given position, the filament cross-section doesn't change over the plotted span in time.

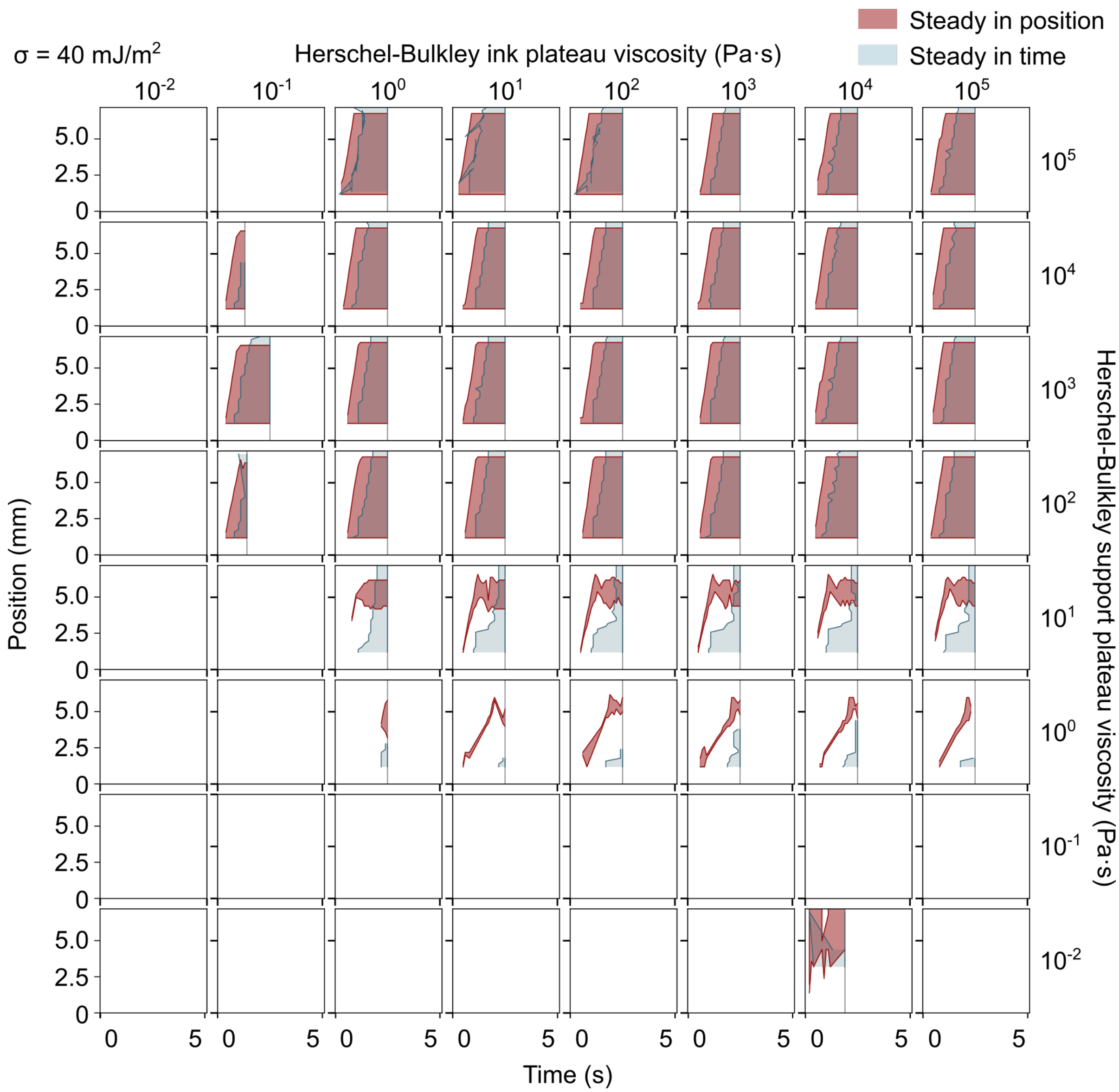

Figure S30: Stability metrics at a surface tension of $40\,\mathrm{mJ/m^2}$, where the ink and support are both Herschel-Bulkley fluids. Stability is defined here using the position of the bottom of the filament. Steady in position means that at a given time, the filament cross-section doesn't change within the plotted span in position. Steady in time means that at a given position, the filament cross-section doesn't change over the plotted span in time.

S7 Viscosity maps

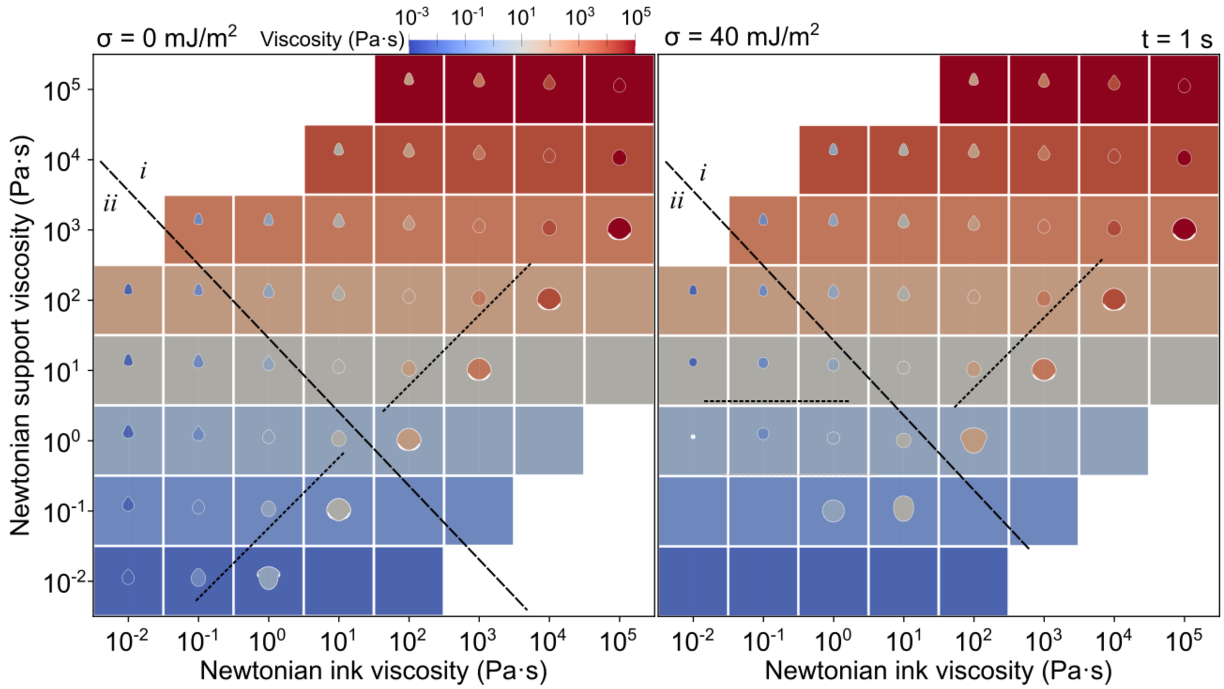

Figure S31: x slices in viscosity, 1.5 mm behind the nozzle after 1 s, where both the ink and support are Newtonian.

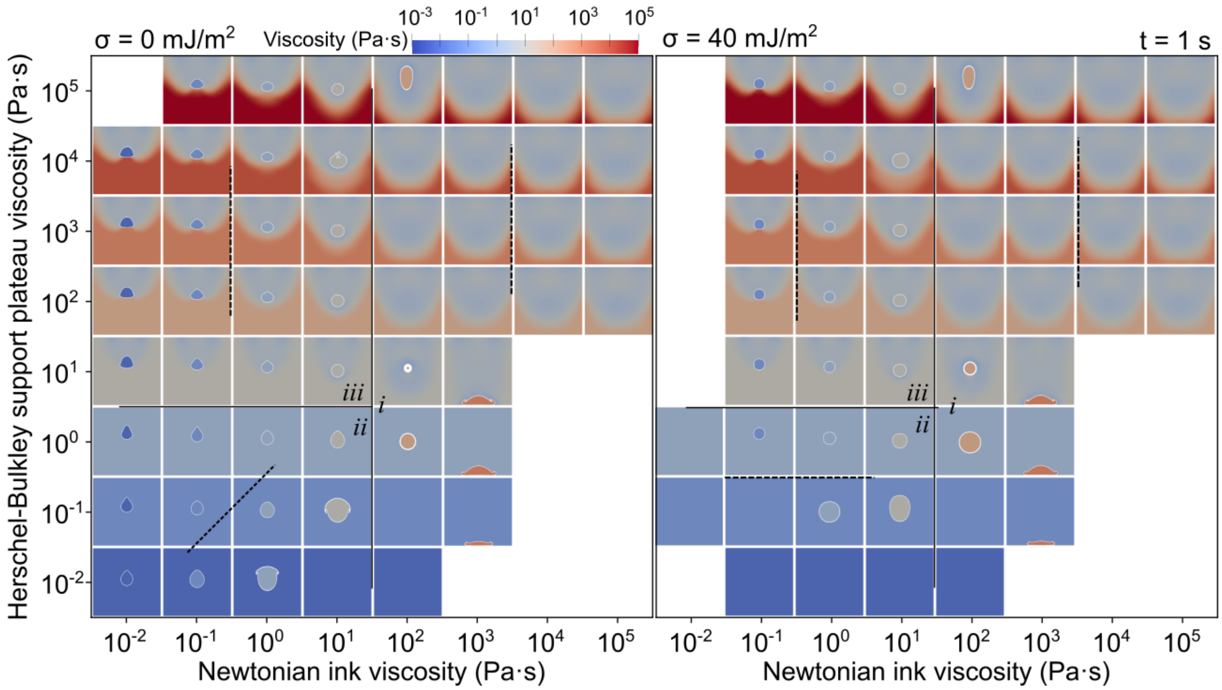

Figure S32: x slices in viscosity, 1.5 mm behind the nozzle after 1 s, where the ink is Newtonian, and the support is Herschel-Bulkley

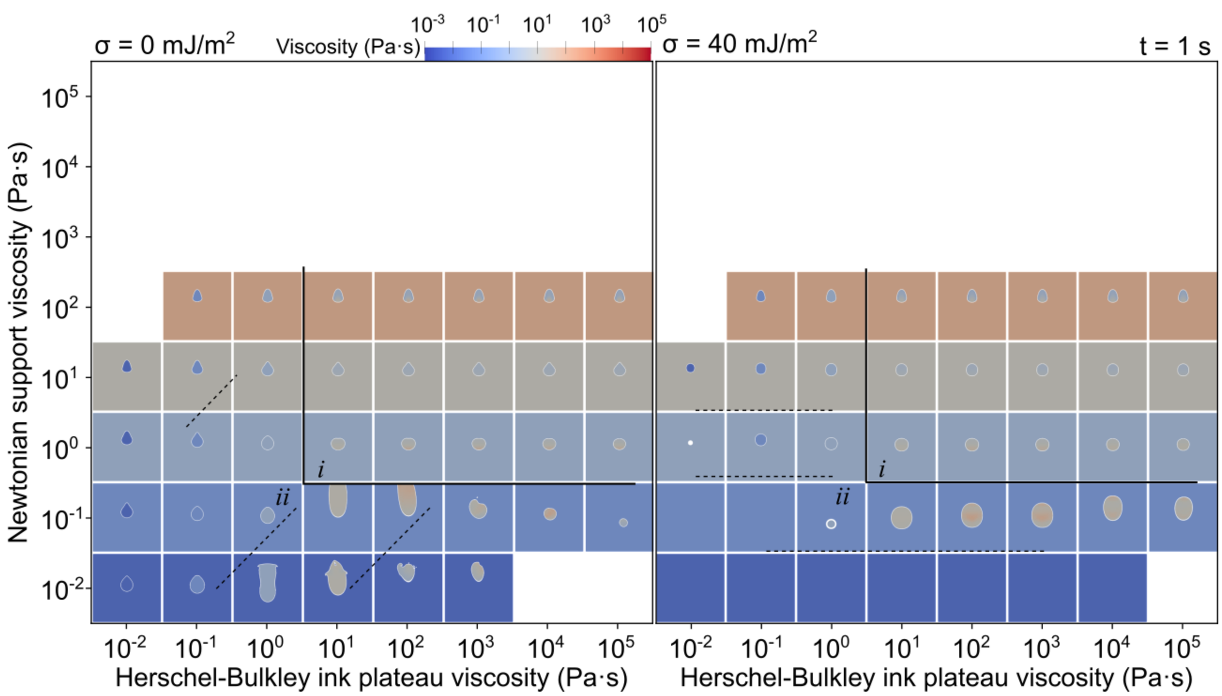

Figure S33: x slices in viscosity, 1.5 mm behind the nozzle after 1 s, where the ink is Herschel-Bulkley, and the support is Newtonian.

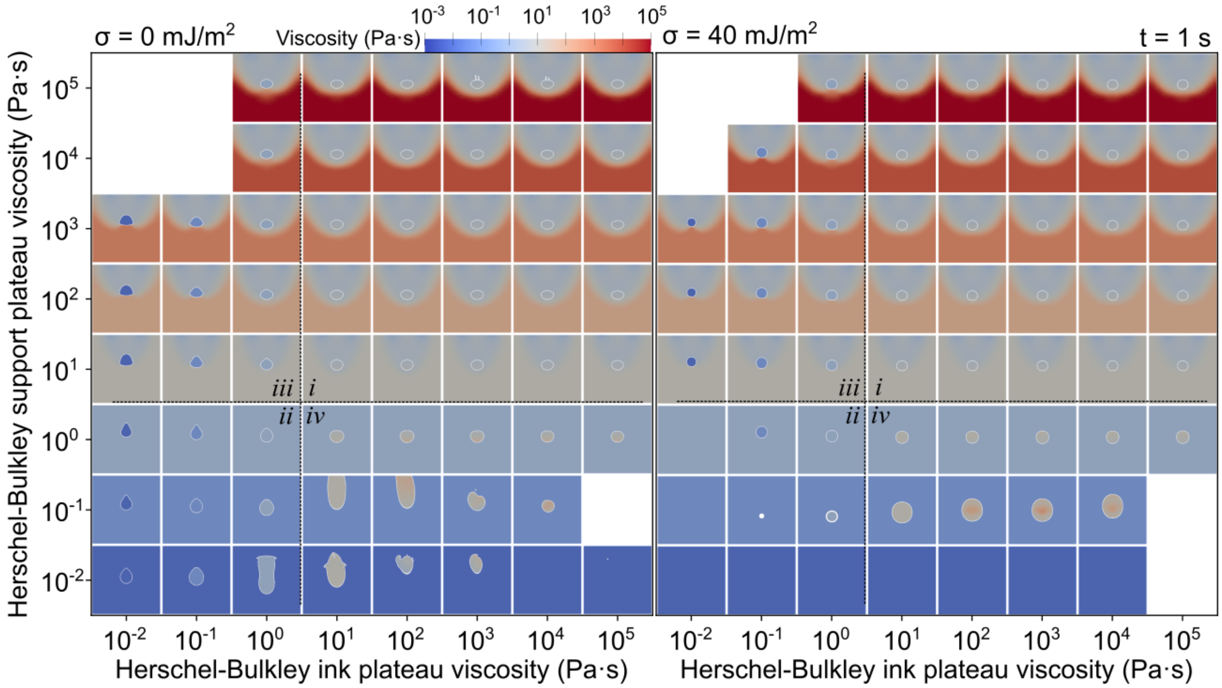

Figure S34: x slices in viscosity, 1.5 mm behind the nozzle after 1 s, where both the ink and support are Herschel-Bulkley.

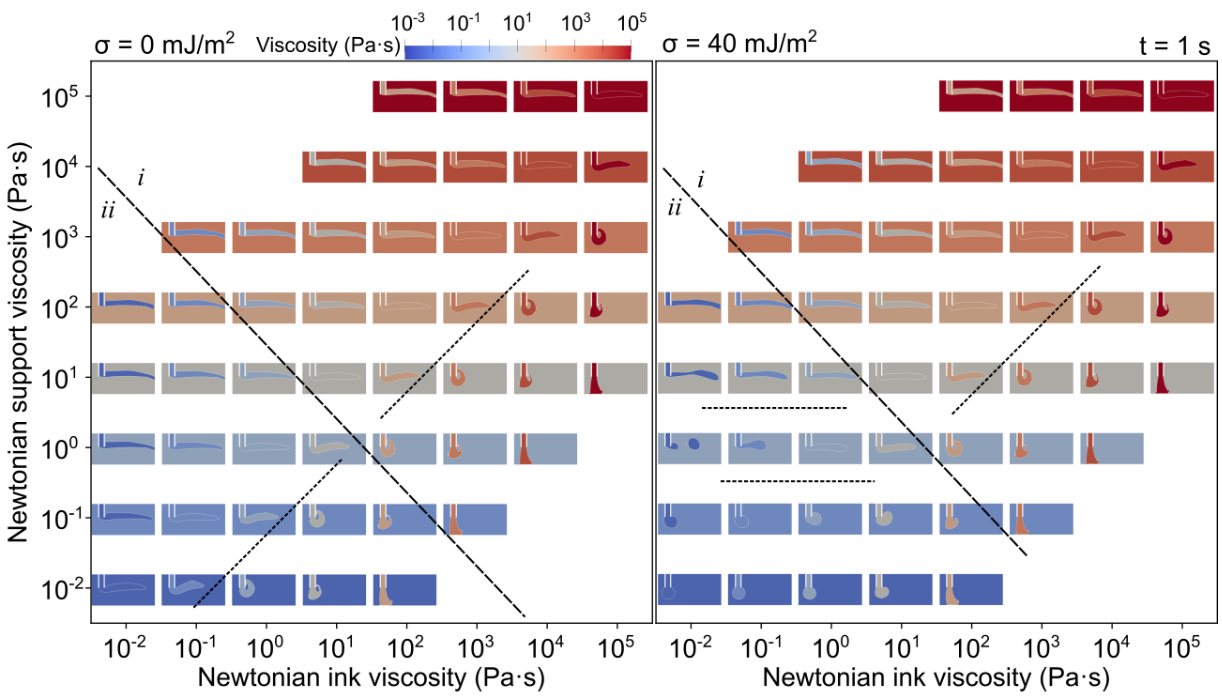

Figure S35: y slices in viscosity, 1.5 mm behind the nozzle after 1 s, where both the ink and support are Newtonian.

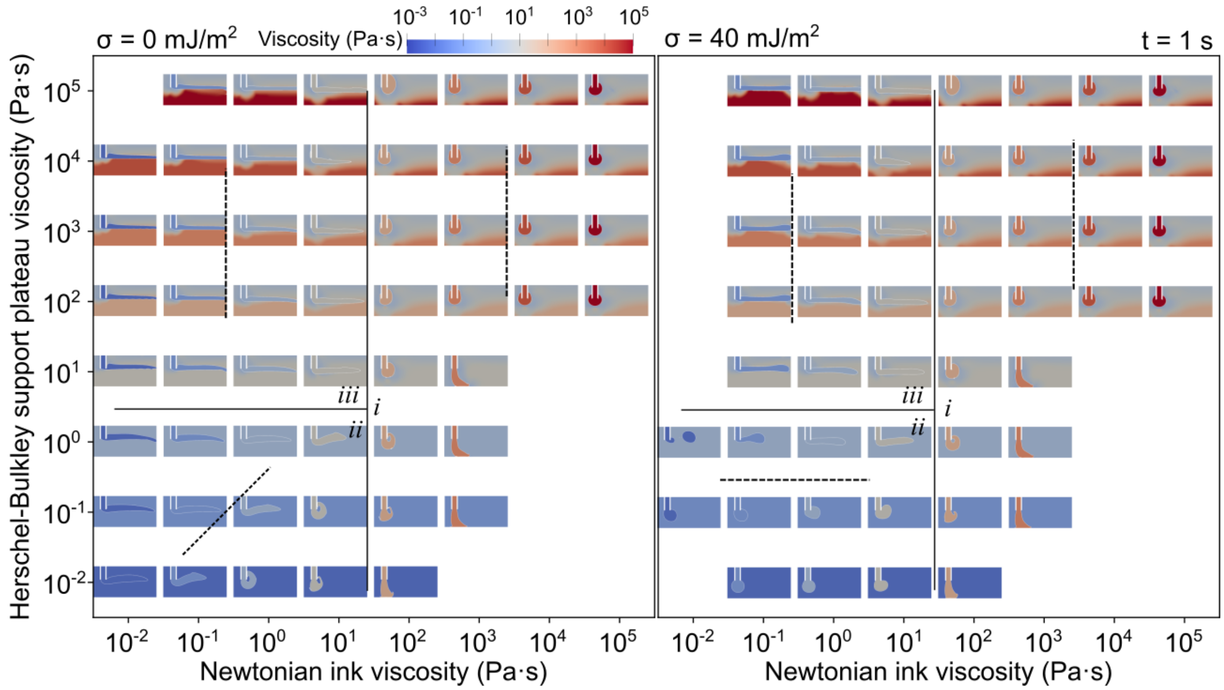

Figure S36: y slices in viscosity, 1.5 mm behind the nozzle after 1 s, where the ink is Newtonian, and the support is Herschel-Bulkley

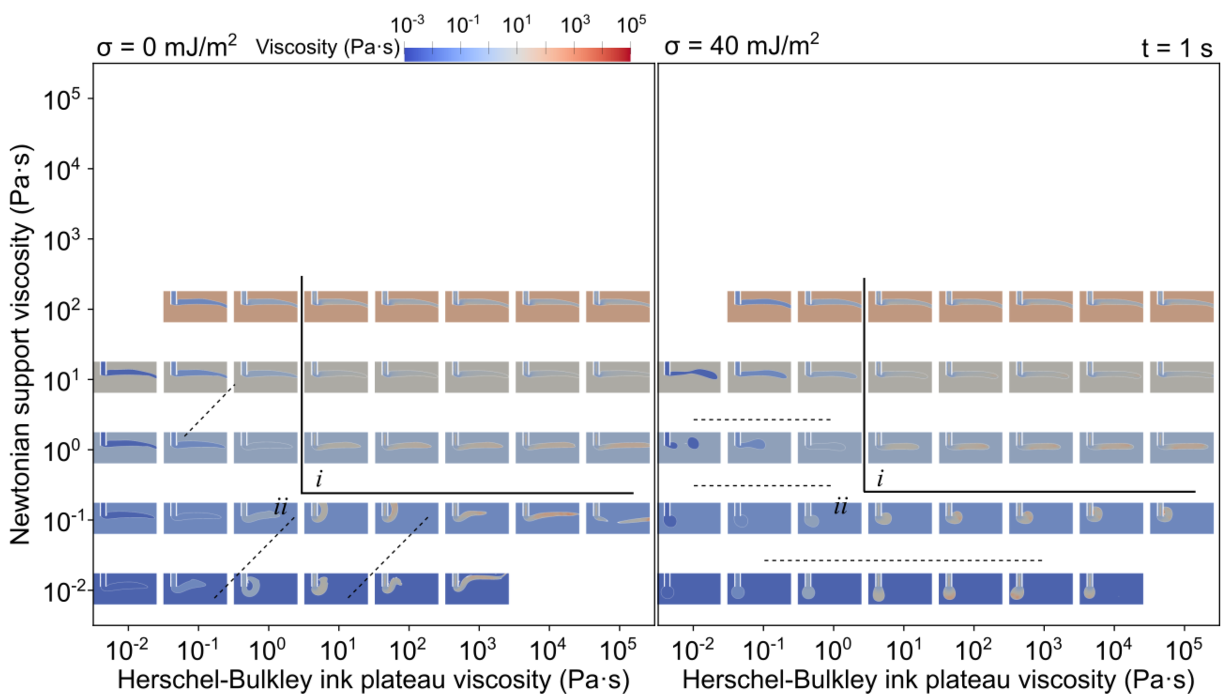

Figure S37: y slices in viscosity, 1.5 mm behind the nozzle after 1 s, where the ink is Herschel-Bulkley, and the support is Newtonian.

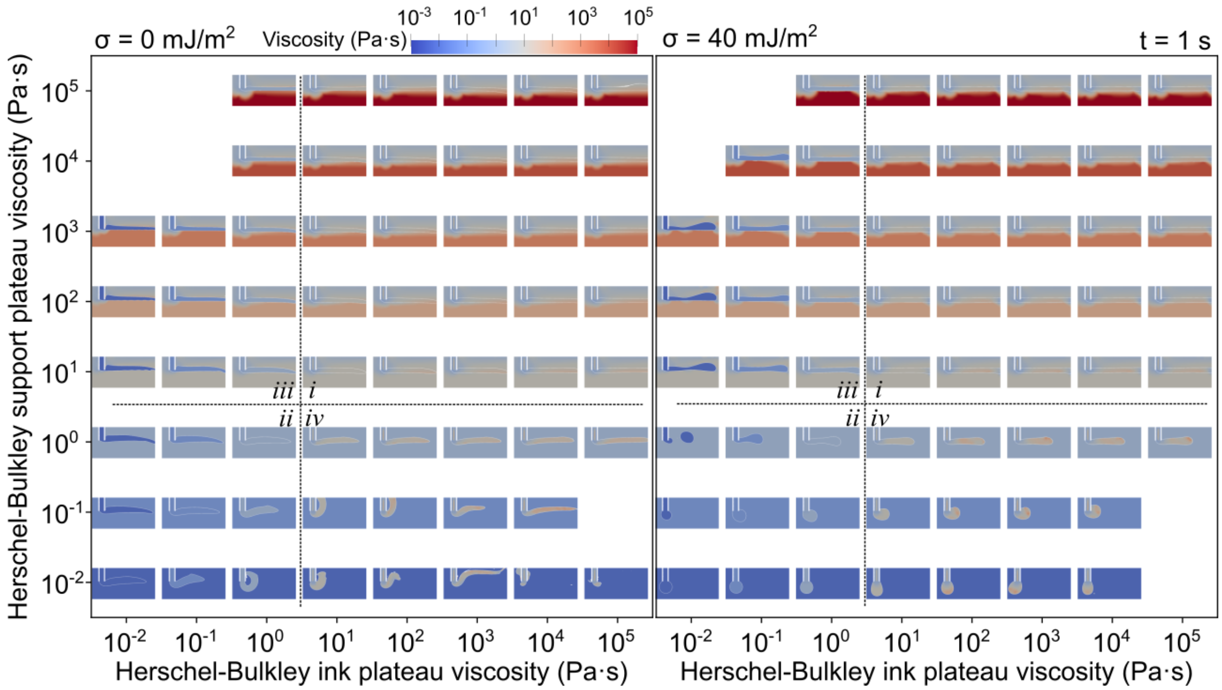

Figure S38: y slices in viscosity, 1.5 mm behind the nozzle after 1 s, where both the ink and support are Herschel-Bulkley.

S8 Velocity maps

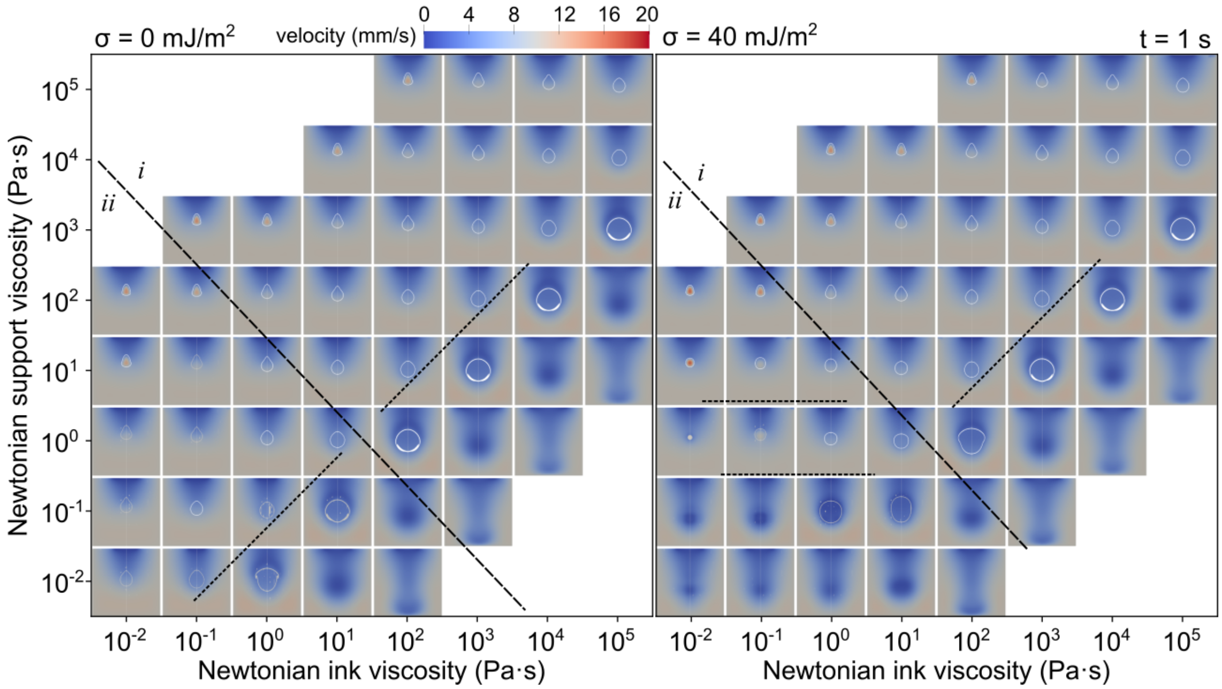

Figure S39: x slices in velocity, 1.5 mm behind the nozzle after 1 s, where both the ink and support are Newtonian.

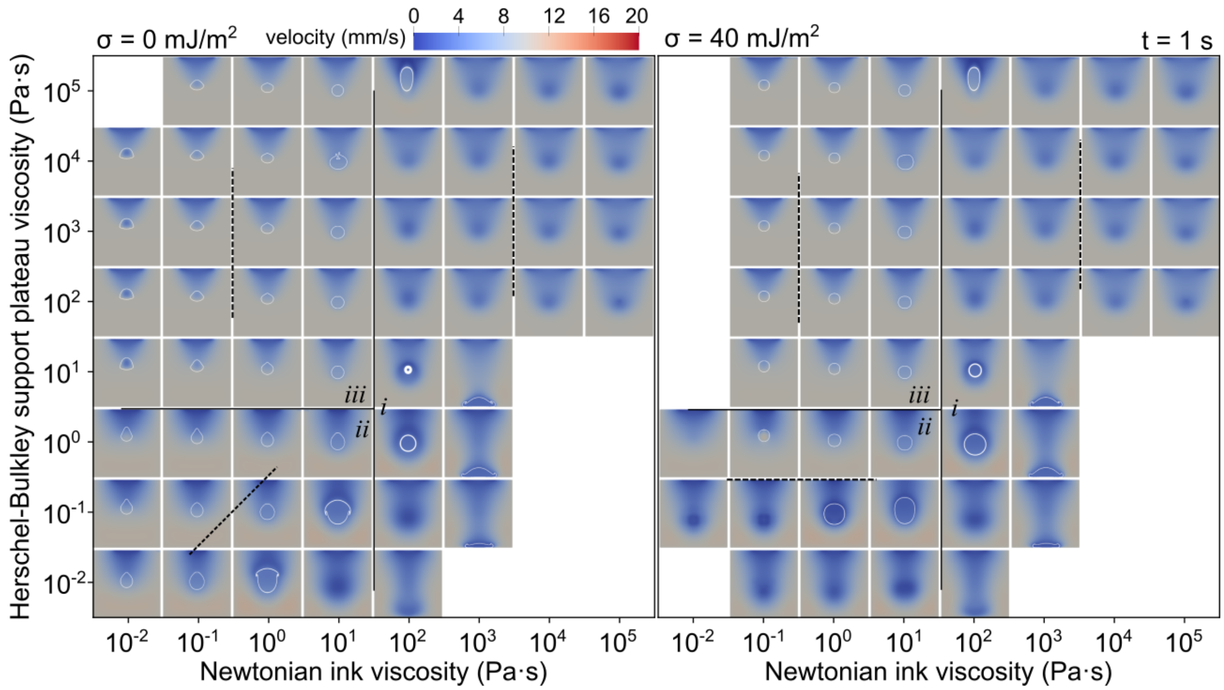

Figure S40: x slices in velocity, 1.5 mm behind the nozzle after 1 s, where the ink is Newtonian, and the support is Herschel-Bulkley

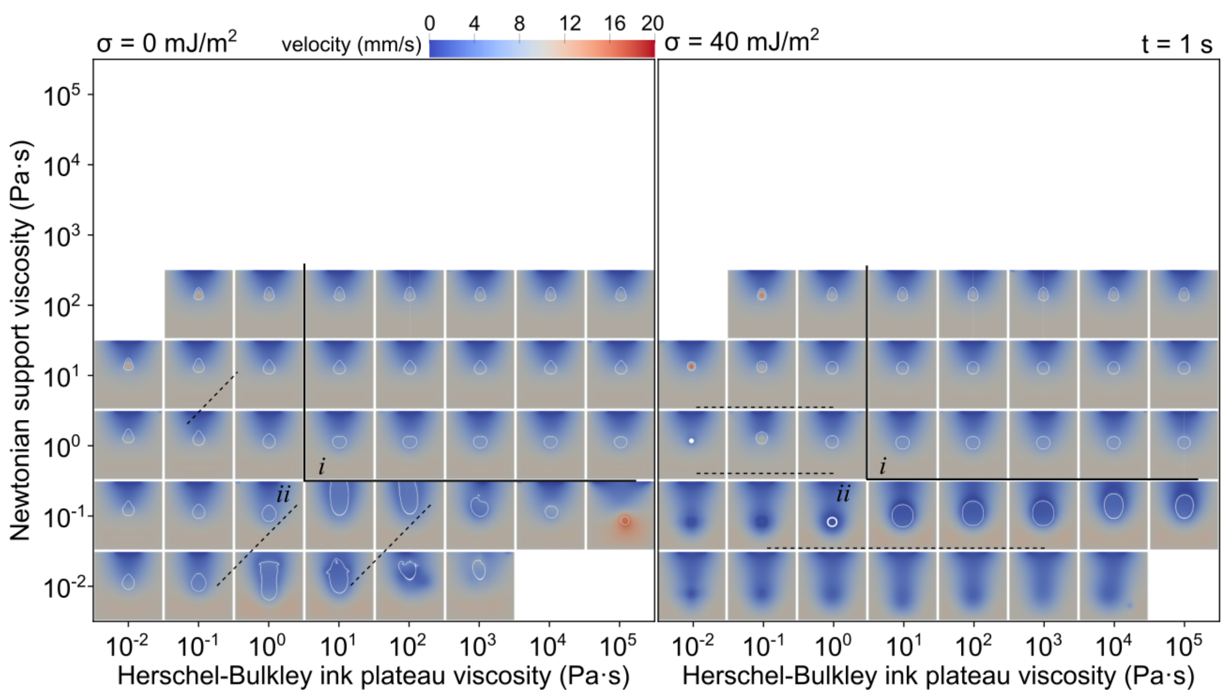

Figure S41: x slices in velocity, 1.5 mm behind the nozzle after 1 s, where the ink is Herschel-Bulkley, and the support is Newtonian.

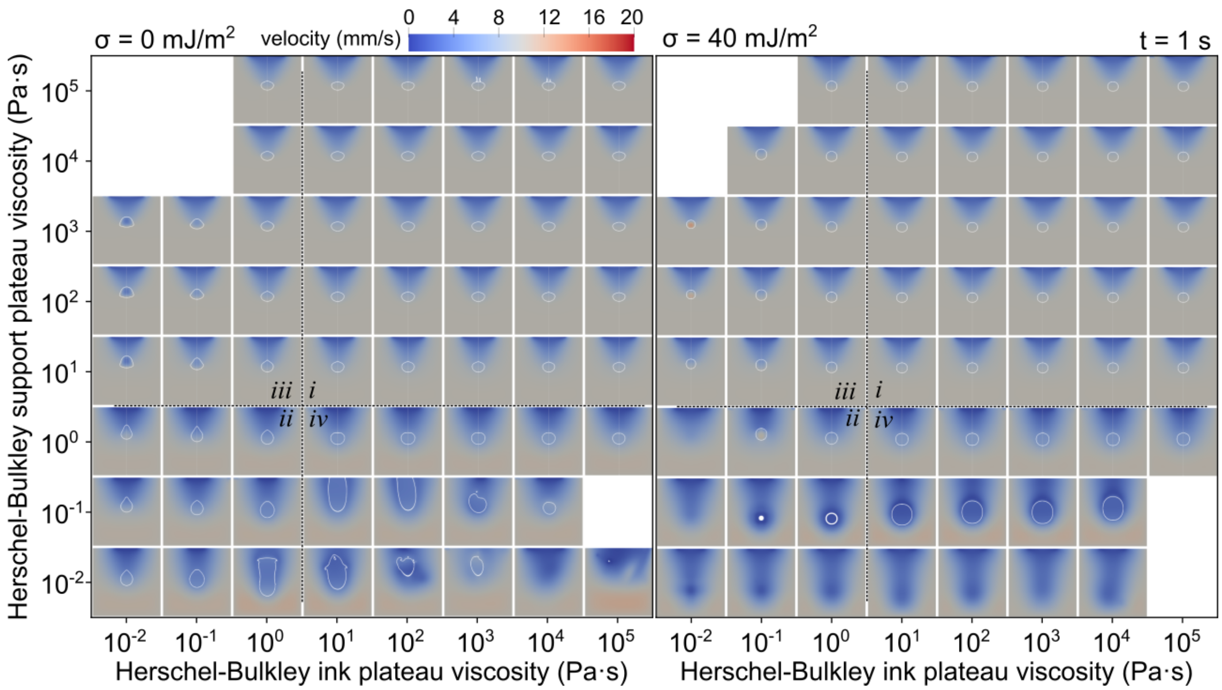

Figure S42: x slices in velocity, 1.5 mm behind the nozzle after 1 s, where both the ink and support are Herschel-Bulkley.

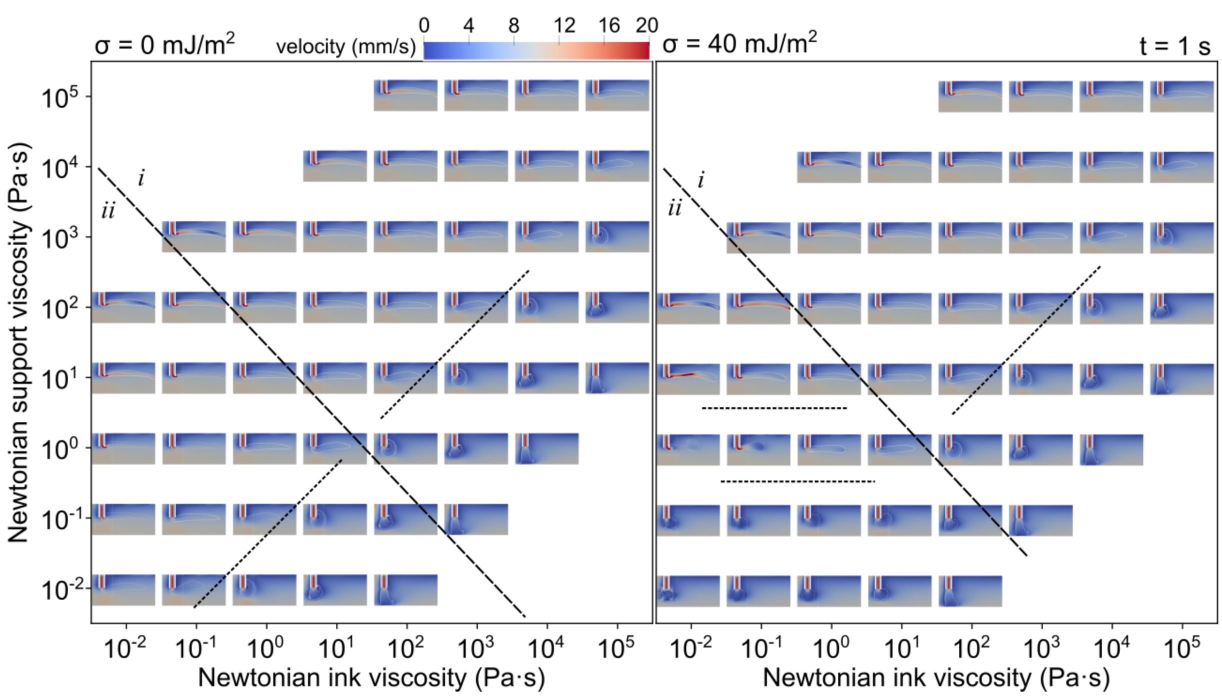

Figure S43: y slices in velocity, 1.5 mm behind the nozzle after 1 s, where both the ink and support are Newtonian.

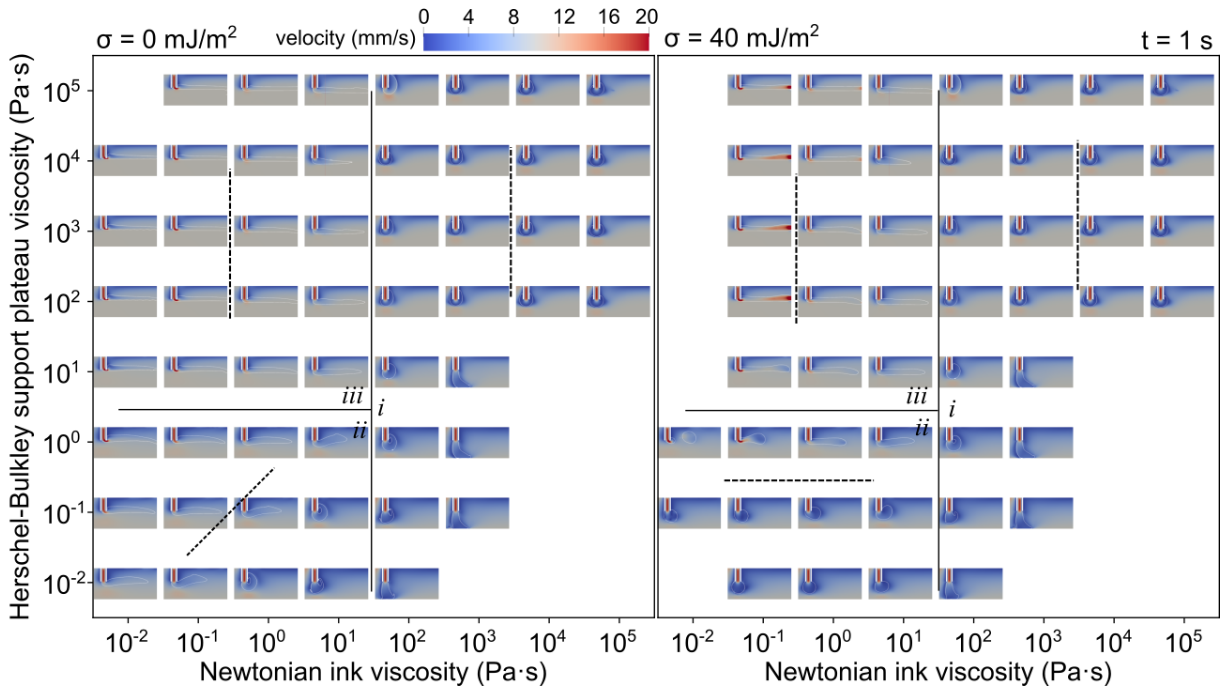

Figure S44: y slices in velocity, 1.5 mm behind the nozzle after 1 s, where the ink is Newtonian, and the support is Herschel-Bulkley

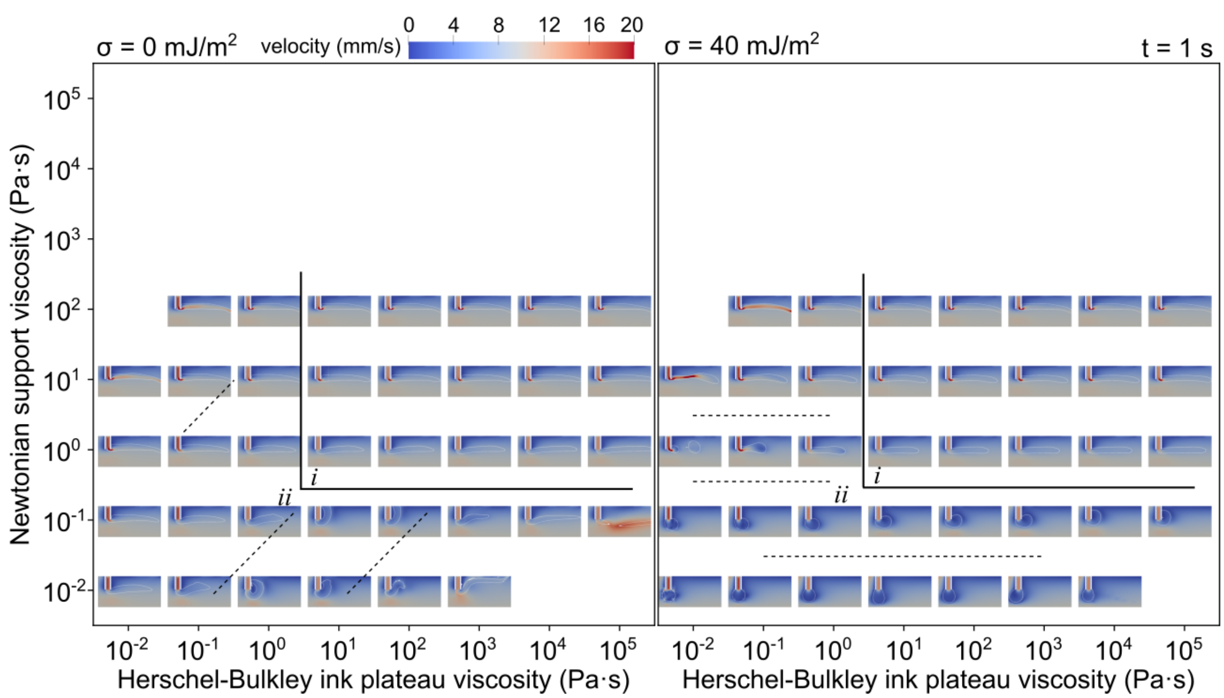

Figure S45: y slices in velocity, 1.5 mm behind the nozzle after 1 s, where the ink is Herschel-Bulkley, and the support is Newtonian.

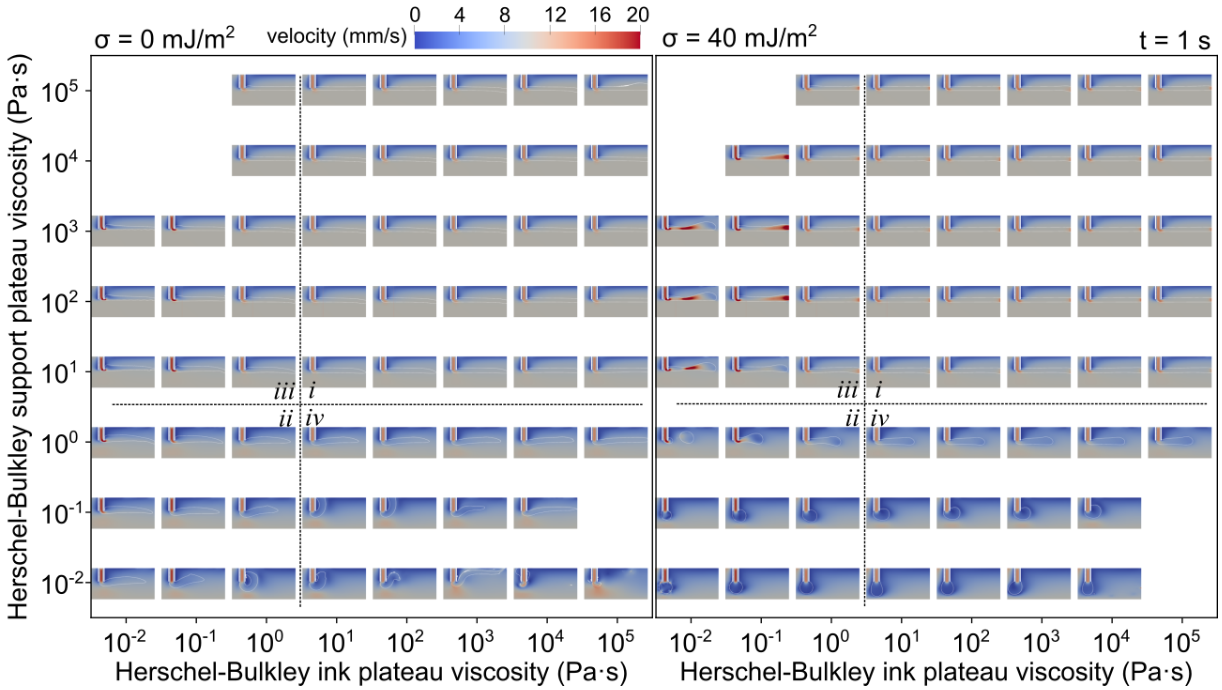

Figure S46: y slices in velocity, 1.5 mm behind the nozzle after 1 s, where both the ink and support are Herschel-Bulkley.

S9 Transients

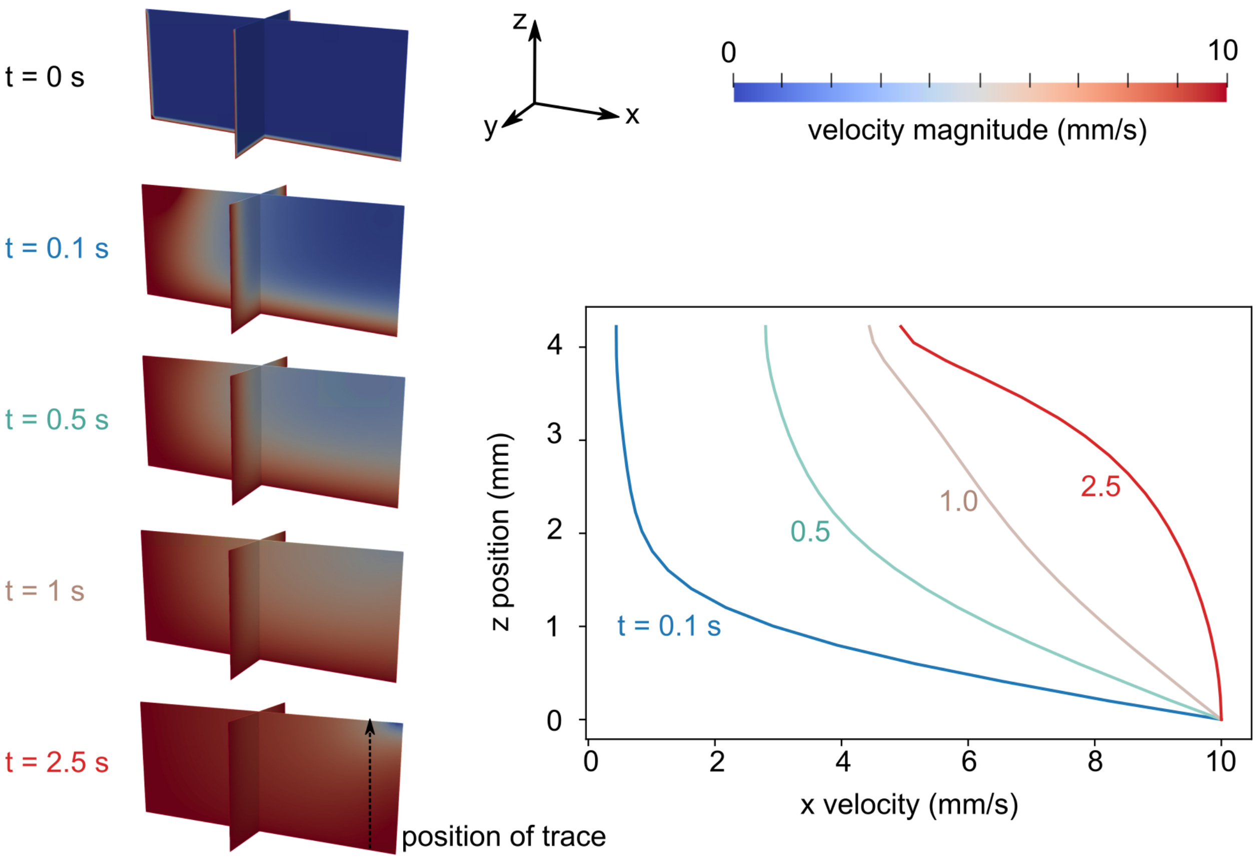

Figure S47: Cross-sections of the bath velocity over time, where there is no nozzle. Plot shows line traces 5.5 mm behind the nozzle, in the y center of the bath, from the bottom to the top of the bath, for Newtonian bath of viscosity 100 Pa·s.

S10 Streamlines

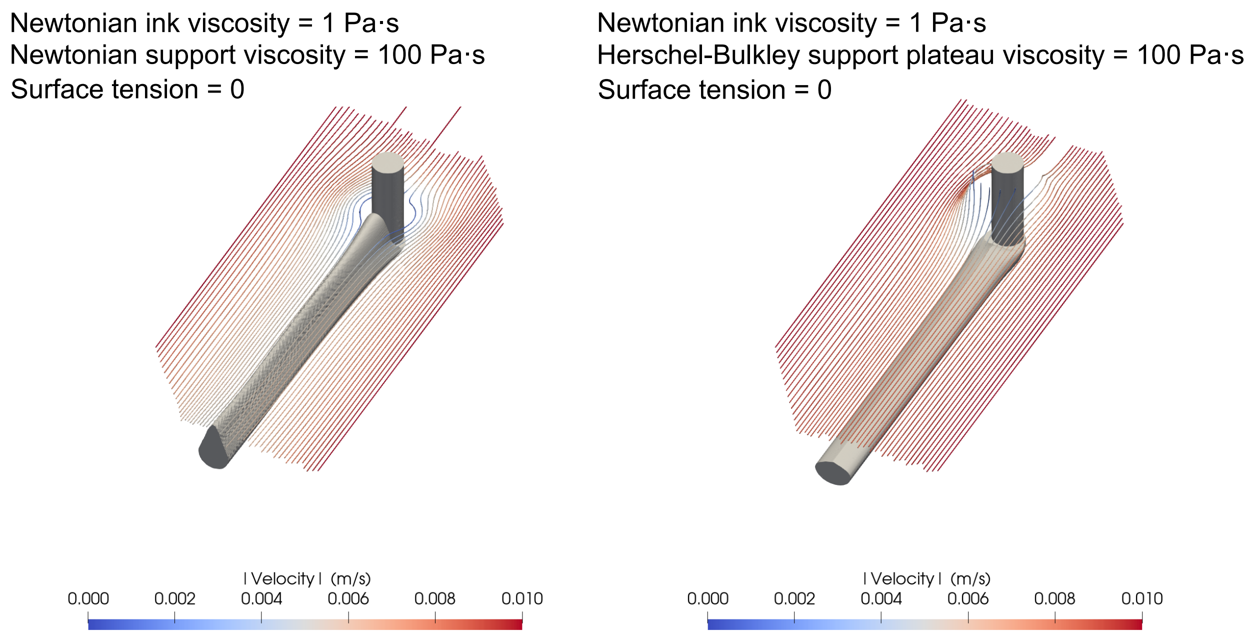

Figure S48: Streamlines around the nozzle, with extruded filament shown, after 2.5 s of flow, at zero surface tension, where the Newtonian ink viscosity is 1 Pa·s, and the Newtonian or Herschel-Bulkley support plateau viscosity is 100 Pa·s. Streamlines pass through the plane 1 mm above the intended center of the filament.

S11 Extrapolating cross-sections

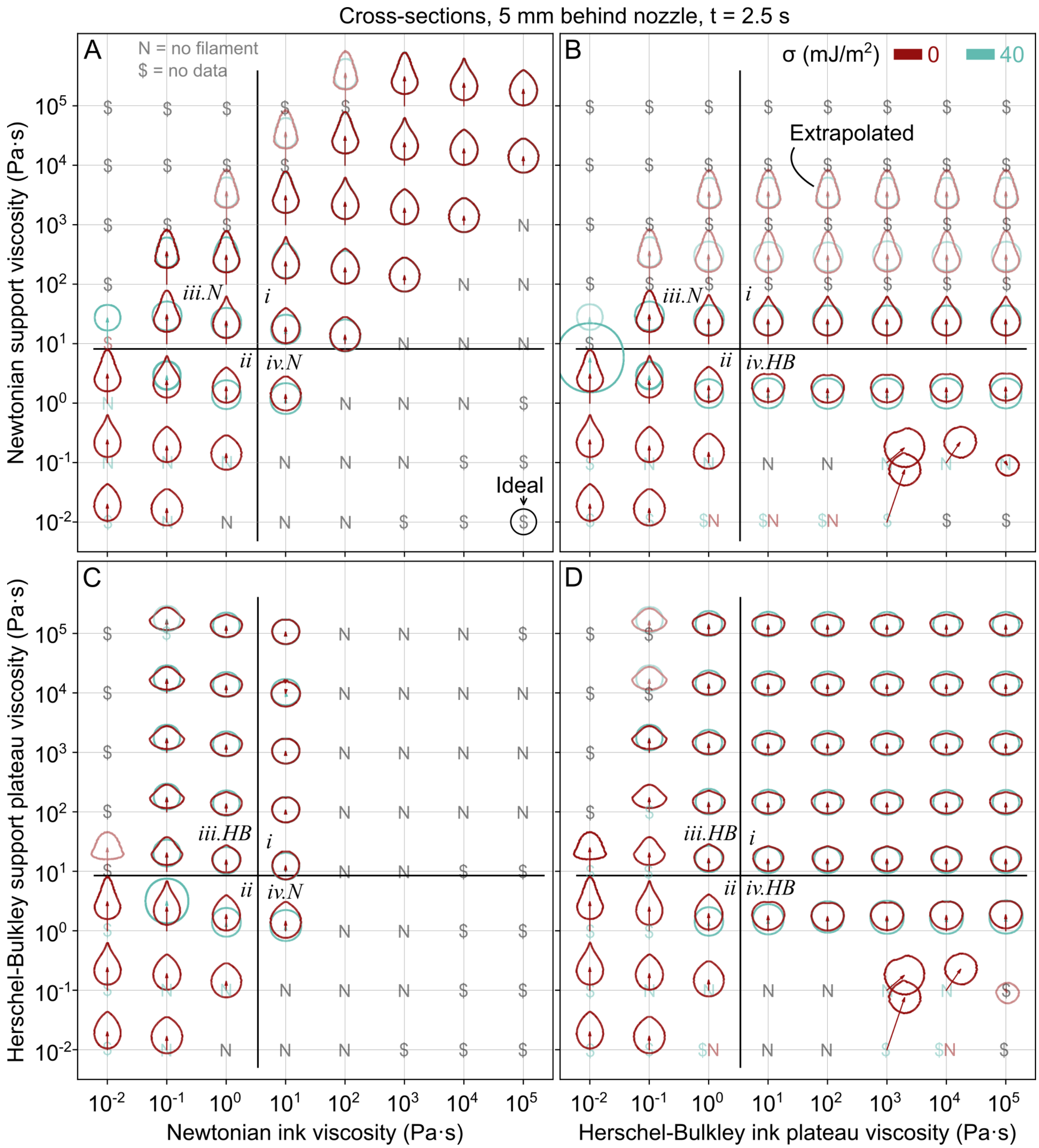

Figure S49: Extrapolated cross-sections, based on trends in the four quadrants. Guesses are shown at 50 % transparency.

S12 Capillary numbers

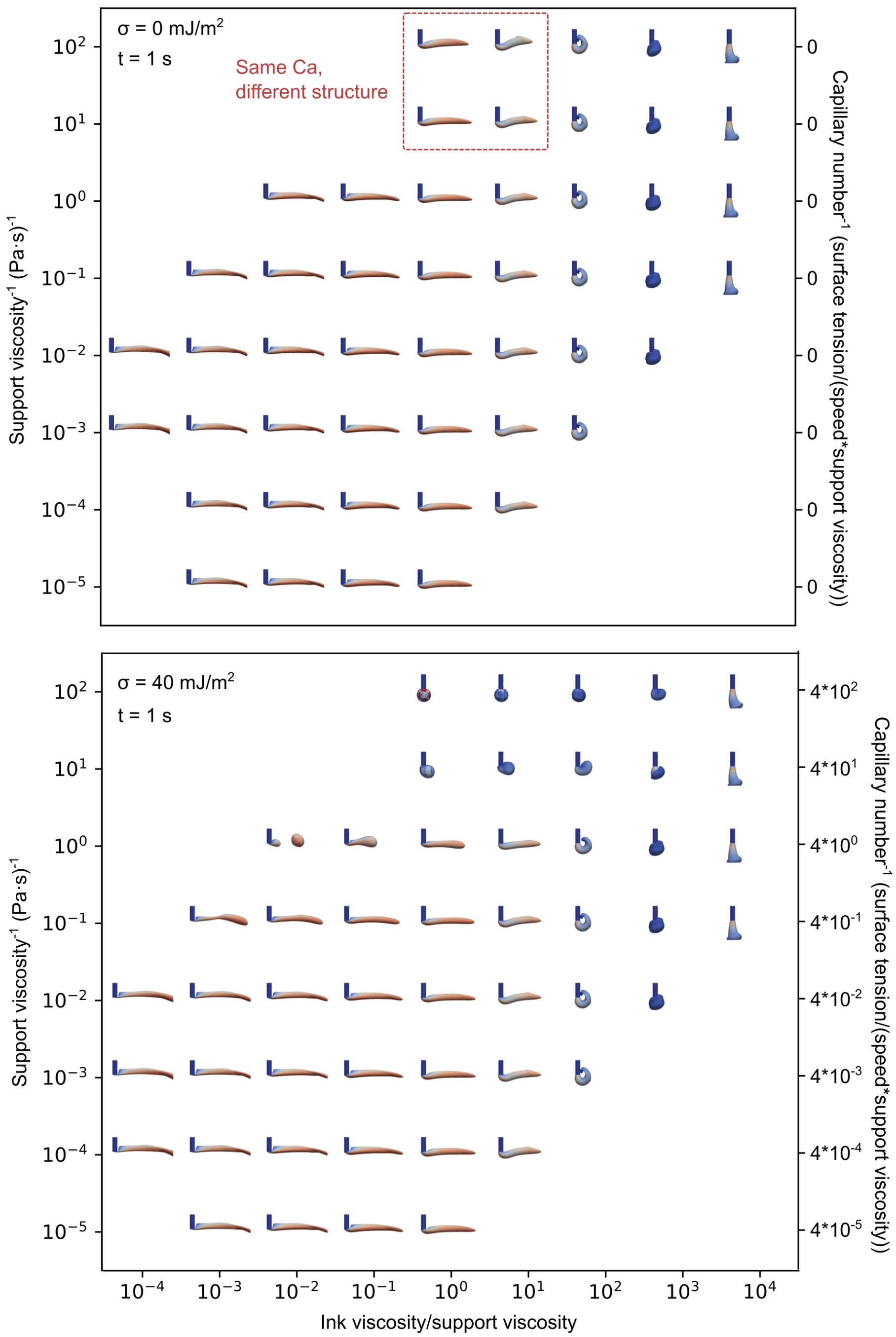

Figure S50: Views of extruded filaments from the $+y$ direction after 1 s of extrusion, where the support is Newtonian. Surfaces indicate the interpolated interface between ink and support, where the volume fraction of ink is 0.5. Colors indicate the magnitude of the velocity at the interface. Blue vertical cylinders represent the ink inside of the nozzle. Results are plotted as the viscosity ratio vs. the inverse support viscosity, which maps onto the inverse capillary number, which is the surface tension divided by the product of the support viscosity and the print speed.

References

[1] Compaan AM, Song K, Huang Y. Gellan Fluid Gel as a Versatile Support Bath Material for Fluid Extrusion Bioprinting. ACS Applied Materials & Interfaces. 2019;11:5714–5726.

[2] Afghah F, Altunbek M, Dikyol C, Koc B. Preparation and characterization of nanoclay-hydrogel composite support-bath for bioprinting of complex structures. Scientific Reports. 2020;10:5257.

[3] Ahlfeld T, Köhler T, Czichy C, Lode A, Gelinsky M. A Methylcellulose Hydrogel as Support for 3D Plotting of Complex Shaped Calcium Phosphate Scaffolds. Gels. 2018;4(3):68.

[4] Ayan B, Zhang Z, Celik N, Zhou K, Wu Y, Costanzo F, et al. Aspiration-assisted Freeform Bioprinting of Tissue Spheroids in a Yield-stress Gel. bioRxiv. 2020;.

[5] Bhattacharjee T, Zehnder SM, Rowe KG, Jain S, Nixon RM, Sawyer WG, et al. Writing in the granular gel medium. Science Advances. 2015;1(8):e1500655.

[6] Cai L, Marthelot J, Brun P. An unbounded approach to microfluidics using the Rayleigh – Plateau instability of viscous threads directly drawn in a bath. Proceedings of the National Academy of Sciences. 2019;116(46):22966–22971.

[7] Cain JD, Azizi A, Maleski K, Anasori B, Glazer EC, Kim PY, et al. Sculpting Liquids with Two-Dimensional Materials: The Assembly of Ti3C2Tx MXene Sheets at Liquid–Liquid Interfaces. ACS Nano. 2019;13(11):12385–12392.

[8] Compaan AM, Song K, Chai W, Huang Y. Cross-Linkable Microgel Composite Matrix Bath for Embedded Bioprinting of Perfusable Tissue Constructs and Sculpting of Solid Objects. ACS Applied Materials & Interfaces. 2020;.

[9] Grosskopf A, Truby R, Kim H, Perazzo A, Lewis JA, Stone HA. Viscoplastic Matrix Materials for Embedded 3D Printing. ACS Applied Materials & Interfaces. 2018;10(27):23353–23361.

[10] Highley CB, Rodell CB, Burdick JA. Direct 3D Printing of Shear-Thinning Hydrogels into Self-Healing Hydrogels. Advanced Materials. 2015;27(34):5075–5079.

[11] Hu Sw, Sung Pj, Nguyen TP, Sheng Yj, Tsao Hk. UV-resistant Self-healing Emulsion Glass as a New Liquid-like Solid Material for 3D Printing. ACS Applied Materials & Interfaces. 2020;.

[12] Jin Y, Compaan A, Bhattacharjee T, Huang Y. Granular gel support-enabled extrusion of three-dimensional alginate and cellular structures. Biofabrication. 2016;8(2):025016.

[13] Jin Y, Compaan A, Chai W, Huang Y. Functional Nanoclay Suspension for Printing-Then-Solidification of Liquid Materials. ACS Applied Materials & Interfaces. 2017;9(23):20057–20066.

[14] Jin Y, Liu C, Chai W, Compaan A, Huang Y. Self-Supporting Nanoclay as Internal Scaffold Material for Direct Printing of Soft Hydrogel Composite Structures in Air. ACS Applied Materials and Interfaces. 2017;9(20):17456–17465.

[15] Jin Y, Song K, Gellermann N, Huang Y. Printing of Hydrophobic Materials in Fumed Silica Nanoparticle Suspension. ACS Applied Materials & Interfaces. 2019;11(32):29207–29217.

[16] Karyappa R, Ching T, Hashimoto M. Embedded Ink Writing (EIW) of Polysiloxane Inks. ACS Applied Materials & Interfaces. 2020;12:23565–23575.

[17] Leblanc KJ, Niemi SR, Bennett AI, Harris KL, Schulze KD, Sawyer WG, et al. Stability of High Speed 3D Printing in Liquid-Like Solids. ACS Biomaterials Science and Engineering. 2016;2(10):1796–1799.

[18] Luo G, Yu Y, Yuan Y, Chen X, Liu Z, Kong T. Freeform, Reconfigurable Embedded Printing of All-Aqueous 3D Architectures. Advanced Materials. 2019;31(49):1904631.

[19] Moxon SR, Cooke ME, Cox SC, Snow M, Jeys L, Jones SW, et al. Suspended Manufacture of Biological Structures. Advanced Materials. 2017;29(13).

[20] Nelson AZ, Kundukad B, Wong WK, Khan SA, Doyle PS. Embedded droplet printing in yield-stress fluids. Proceedings of the National Academy of Sciences of the United States of America. 2020;117(11):5671–5679.

[21] O'Bryan CS, Bhattacharjee T, Marshall SL, Sawyer WG, Angelini TE. Commercially available microgels for 3D bioprinting. Bioprinting. 2018;11(August):e00037.

[22] O'Bryan CS, Kabb CP, Sumerlin BS, Angelini TE. Jammed Polyelectrolyte Microgels for 3D Cell Culture Applications: Rheological Behavior with Added Salts. ACS Applied Bio Materials. 2019;2(4):1509–1517.

[23] O'Bryan CS, Bhattacharjee T, Hart S, Kabb CP, Schulze KD, Chilakala I, et al. Self-assembled micro-organogels for 3D printing silicone structures. Science Advances. 2017;3(5):e1602800.

[24] Senior JJ, Cooke ME, Grover LM, Smith AM. Fabrication of Complex Hydrogel Structures Using Suspended Layer Additive Manufacturing (SLAM). Advanced Functional Materials. 2019;29(49):1904845.

[25] Spencer AR, Shirzaei Sani E, Soucy JR, Corbet CC, Primbetova A, Koppes RA, et al. Bioprinting of a Cell-Laden Conductive Hydrogel Composite. ACS Applied Materials and Interfaces. 2019;11(34):30518–30533.

[26] Uchida T, Onoe H. 4D Printing of Multi-Hydrogels Using Direct Ink Writing in a Supporting Viscous Liquid. Micromachines. 2019;10(7):433.

[27] Wu W, Deconinck A, Lewis JA. Omnidirectional printing of 3D microvascular networks. Advanced Materials. 2011;23(24):178–183.

[28] Yu Y, Liu F, Zhang R, Liu J. Suspension 3D Printing of Liquid Metal into Self-Healing Hydrogel. Advanced Materials Technologies. 2017;2(11):1700173.

[29] Zhao J, Hussain M, Wang M, Li Z, He N. Embedded 3D printing of multi-internal surfaces of hydrogels. Additive Manufacturing. 2020;32:101097.